https://ntrs.nasa.gov/search.jsp?R=19830008513 2020-03-21T06:01:58+00:00Z

NASA
CR
3663
c.1

AFWL/SUL
TECHNICAL LIB
KIRTLAND AFB
0062466
TECH LIBRARY KAFB, NM

NASA Contractor Report 3663

Design Concepts for Large Reflector Antenna Structures

John M. Hedgepeth and Louis R. Adams

CONTRACT NAS1-16134
JANUARY 1983

NASA

TECH LIBRARY KAFB, NM

0062466

NASA Contractor Report 3663

Design Concepts for Large Reflector Antenna Structures

John M. Hedgepeth and Louis R. Adams
Astro Research Corporation
Carpinteria, California

Prepared for
Langley Research Center
under Contract NAS1-16134

National Aeronautics
and Space Administration

Scientific and Technical
Information Branch

1983

TABLE OF CONTENTS

ABSTRACT 1

INTRODUCTION 1

APPROACHES TO THE ERECTION OF LARGE TRUSS STRUCTURES IN SPACE 3

- Sequential Erection 4
- Approaches Using Solid Reflector Panels 4
- Approaches Using a Compliant Mesh Reflector 6
- Selection of Concept for Further Study 8

A NEW APPROACH TO THE DEPLOYMENT OF TETRAHEDRAL TRUSSES 9

- Deployment Schematic 10
- Sequentially Deployed Tetrahedral Truss 11
- Joint Design 12
- Example Hinge Geometry 15

DESIGN AND FABRICATION OF MODELS 18

- Concept Visualization Model 18
- High Fidelity Model 19
  - Engineering and Design 19
  - Materials 20
  - Fabrication 21
  - Assembly 21
  - Transition Forces 21
  - Weights 22

DESIGN OF DOUBLY CURVED REFLECTORS 22

- Geometrical Analysis for Quasi-Sphere 24
- Numerical Examples 30

NATURAL VIBRATION OF SHALLOW SHELLS 31

- Differential Equations 32
- Boundary Conditions 32
- Solutions 33

CONCLUDING REMARKS 37

REFERENCES 38

LIST OF ILLUSTRATIONS

Table 1. Fortran computer program for quasisphere geometry 39
Table 2. Example interactive session 42
Table 3. Joint geometry of quasispherical tetratruss 48

Figure 1. Tetrahedral truss reflector structure 51
Figure 2. Assembly of surface panels to erected truss 52
Figure 3. Assembly from deployable modules 53
Figure 4. Astrocell module 54
Figure 5. Intermodule connections 55
Figure 6. Deployable solid panel integrated truss 56
Figure 7. Diameter of constant-curvature spherical segments required for a 30-meter-diameter paraboloidal reflector to operate at various frequencies 57
Figure 8. Pretensioned truss configuration 58
Figure 9. Tetrahedral truss configuration 59
Figure 10. 200-meter-diameter deployable antenna 60
Figure 11. Schematic diagram of sequential deployment 61
Figure 12. Tetrahedral truss structure showing joint locations 62
Figure 13. Tetrahedral truss nomenclature 63
Figure 14. Partially deployed structure 64
Figure 15. Second-stage deployment 65
Figure 16. Surface-member packaging 66
Figure 17. Coordinates and angles 67
Figure 18. Detail of concept visualization model 68
Figure 19. Deployment sequence of a sequentially deployable tetrahedral truss structure 69
Figure 20. Almost-over-center hinge 72
Figure 21. Nine-member joint 73
Figure 22. Hinge details 74
Figure 23. Deployment sequence 75
Figure 24. Geometry and nomenclature for doubly curved truss 76
Figure 25. The influence of curvature on the natural frequencies of a shallow spherical shell with a free circular edge for two waves around the circumference and circumferential mode numbers s of 0, 1, and 2 77

DESIGN CONCEPTS FOR LARGE REFLECTOR ANTENNA STRUCTURES

ABSTRACT

Practical approaches for establishing large, precise antenna reflectors in space are described. Reflector surfaces consisting of either solid panels or knitted mesh are considered. The approach using a deep articulated truss structure to support a mesh reflector is selected for detailed investigation. A new sequential deployment concept for the tetrahedral truss is explained. Good joint design is discussed, and examples are described both analytically and by means of demonstration models. The influence of curvature on the design and its vibration characteristics are investigated.

INTRODUCTION

Future economic use of space will require large antennas for a variety of uses. The reflector antenna has advantages of high efficiency, potential low cost and unit weight of the large-aperture portion (the reflector), and broadband capability. On the other hand, the reflector is required to be of much greater precision than a lens and is not capable of easy local electrical phase adjustment as is a phased array. There is, therefore, a need for large spaceborne reflector structures which can yield high accuracy.

Large antennas are needed in order to handle large amounts of radiofrequency power (high gain) and to concentrate the region of reception or transmission into a narrow beam (low side lobes). Both of these objectives demand high accuracy. For those missions for which the on-axis gain is of primary importance, the rms error of the wavefront should be held to less than 12 percent of the wavelength. For those astronomical and Earthward-pointing missions in which the side-lobe gain must be kept very low and in which loss of power from the main lobe is undesirable, the rms wavefront error should be less than 4 percent of the wavelength.

In a reflector antenna the wavefront error is approximately equal to twice the geometrical error measured normal to the reflector surface. Thus, the surface error of a reflector must be held to about one-fifteeth of a wavelength for the more demanding missions.

The difficulty of erecting antennas is dependent on the relation between the allowable error and the aperture. Very few missions require less accuracy than one ten-thousandth of the diameter, and demands for an rms surface error of less than one-millionth of the diameter are not uncommon. As an intermediate example, good communication at C-band (wavelength $\simeq$ 5 cm) requires a surface rms accuracy of 1 mm. A 100-m-diameter antenna, which would concentrate its beam on a 18-km-sized spot on the Earth from geosynchronous orbit, has an allowable error of one part in 100,000.

Achieving the required accuracy for a reflector antenna in space can be a difficult task. While it is theoretically possible to do this by periodically (or continuously) measuring the surface and adjusting it to bring it to the correct shape, the mechanization is complicated and expensive. A more practical approach is to provide a structure of sufficient stiffness and dimensional stability that no unacceptable distortions occur during the operational lifetime. Such a "passive-structure" approach is attractive for its relative simplicity and its more easily achieved reliability. Its attractiveness is even further enhanced if the initial adjustment operations in space are minimized or eliminated.

The expected accuracy of prebuilt, passive structures is dependent on materials used, on the structural configuration selected, and on the fabrication and test procedures employed. Clearly, the materials composing the structure must possess high dimensional stability if stringent accuracy requirements are to be met. Similarly, the fabrication/test combination must result in very precise geometry. The burden placed on these factors, however, is determined largely by the choice of structural configuration. The needed accuracy can be attained only if the structure is well designed with straight load paths and if it is made deep enough to avoid excessive curvature due to differential strains across the depth.

The influence of structural configuration on the accuracy of antenna structures has been treated in References 1 and 2. The principal finding is that deep truss structures do indeed have the potential of yielding high

accuracy. In fact, the investigation showed that error/diameter ratios of one part in a million are achievable if the structure is assembled from elements which are made accurately in detail and then joined without further adjustment. The buildup of tolerance error arising from such an approach is small enough if the rms unit error in the length of the elements is 10^{-5}, a fabrication precision achievable at reasonable cost with careful tooling, and if the structure is a fully formed truss such as the tetrahedral truss shown in Figure 1.

The subject of this report is the investigation of practical approaches for establishing in space the type of antenna-reflector structures exemplified in Figure 1. Attention is confined to those approaches that involve deployment from efficiently stowed packages, and possibly include assembly of modules. The various approaches are first described. More detailed treatment is given to the deployable articulated truss with a mesh reflector, inasmuch as this concept offers the most potential of achieving truly large diameters with a single Shuttle payload. Geometrical studies are presented for the design of member lengths and hinge geometries for the sequentially deployed tetrahedral truss. The means of producing a proper doubly curved surface are investigated. Finally, the design and fabrication of models illustrating the concept are discussed.

APPROACHES TO THE ERECTION OF LARGE TRUSS STRUCTURES IN SPACE

The deep-truss type of antenna structure has many advantages, particularly for high-accuracy applications. The reliable establishment of this type of structure in its operational orbit is therefore a desirable objective. Of the many conceivable techniques for constructing truss structures, the ones to be employed in the near future are those of deployment, assembly, or a combination of the two. These approaches, called herein by the term "erection," have the characteristic that most, if not all, of the precise fabrication work is performed before launch into space; the tasks to be performed in space are consequently kept to very simple ones. Thus, even if extravehicular activity by the on-orbit crew were required for the erection in space, the effort and cost would be reasonable. The purpose of this section is to describe some approaches for practical space erection.

Sequential Erection

Before describing individual approaches, it is desirable to establish an important principle affecting concept selection. The truss structures under consideration have many hinges and joints, all of which must operate successfully in order to produce a properly erected structure. Clearly, the reliability of the erection is of primary concern. Acceptable reliability can only be achieved by assuring extremely high reliability for the individual operations. Intuitively, a synchronous deployment of all joints is difficult to make high in reliability. The difficulties of management of internal forces during deployment, of spatial control of the various members, and of the provision of well simulated ground tests are some of the barriers to high reliability for synchronous deployment. The alternative is some form of sequential erection.

Sequential erection obeys the following rules:

1. Most of the material is either securely stowed or fully erected at any time during the period of erection.
2. Only a small part of the material is in transition at any time.
3. Parts in transition are carefully controlled.

Obeying the principle of sequential erection allows attention to be concentrated on those parts in transition. It allows a close approach to the ideal of being able to control the actuation of the joints individually and repetitively. If a malfunction does occur, sequential erection allows the possibility of inspection, analysis, and repair so that the erection can be continued.

Note that the Astromast™, a highly successful, intricate deployable lattice boom, follows this principle. So do the so-called furlable booms, such as the STEM™ (Storable Tubular Extendible Member) and TEE™. And, in fact, so does on-orbit assembly, which is considered by many to be a desirable method for space erection. The advantages of sequential erection are impressive; most of the concept approaches described herein therefore follow the principle.

Approaches Using Solid Reflector Panels

Attractive structural configurations depend primarily on the characteristics of the payload - in this case, the reflector surface. If the reflector

is made up of solid panels, the structure has the task of holding the panels in proper relation to each other. The panels can be shaped individually to yield a highly accurate assembly.

One approach is illustrated in Figure 2. Here the reflector panels are mounted on a previously erected truss structure. The truss could be assembled from individual struts, from deployed modular cells, or deployed from a single package by the technique described in a following section.

A more nearly integrated approach is to attach the structural modules to their reflector panels, deploy each module, and assemble as shown in Figure 3. The module's shape and stowed configuration are selected to utilize the Shuttle payload volume efficiently. The panel is preattached to the structure at three points which could include means for adjusting the position of the panel.

A working scale model of a possible structural module - the "Astrocell" - is shown in Figure 4. The structure consists of the upper and lower triangular frames and the diagonals. The curved "longerons" are not part of the primary structure; they are prebuckled and therefore supply the forces necessary to pretension the diagonals. The module is capable of carrying compression with full stiffness. The design of the hinges and other attachments has been carefully thought out so as to achieve maximum compactness. The depth of the packaged module is just the sum of the triangular-frame thicknesses and the panel depth. The deployment motion is quite similar to that of one bay of an Astromast lattice column.

The joints between modules must provide a good structural tie. They often must also provide for electrical connections. One concept for meeting these requirements is shown in Figure 5. The probe-and-drogue arrangement facilitates engagement, and a torqued fastener on the end of the probe precompresses the joint. Modularity is enhanced by providing the universal triangular transition piece in which the variations in electrical circuitry (which is often present in practical hardware) can be accommodated.

The foregoing approaches require assembly operations which place severe requirements on the assembly mechanisms; large distances must be covered, and the final mating is relatively precise. An approach that avoids this is to hinge adjacent modules together insofar as possible and package them together

in a container that incorporates a preprogrammed deployment mechanism which will first deploy the next module, then rotate itself and the module into the proper position, and, finally, fix the mated joints. The restraint furnished by the hinge, together with the local stiffness of the module elements, makes the targeting task possible even with relatively crude actuators. An example of this approach is shown in Figure 6.

The erection of reflectors using solid panel modules would be especially cost effective if all the panels had the same shape. Then the reflector could be composed of similar elements built on common tooling, and the economies of quantity production could be achieved. Unfortunately, the desired surface is usually paraboloidal rather than spherical. The possibility exists of making the paraboloid from properly positioned spherical panels, all of which have the same shape. The error between the desired surface and the spherical segments is kept small enough by limiting the size of the panels. The resulting restrictions of panel size are shown in Figure 7 (taken from ref. 3).

Using solid reflector panels is attractive, especially when low wavelengths are desired. The size of reflector that can be packaged in a single Shuttle bay is limited, however. For example, assume each module in the configuration of Figure 3 has a packaged thickness of 7 cm. The full length of the Shuttle bay can then hold 220 modules in addition to the deployment mechanisms. The resulting assembled reflector is limited to about 50 m in diameter. Truly large apertures would require multiple launches.

Approaches Using a Compliant Mesh Reflector

An available reflector surface suitable for large deployable antennas is the mesh made of metallic filament knitted or woven into a sheet which can be stretched over the surface grid supplied by the structural truss. Such a mesh provides good reflection when stretched and is able to be folded compactly for launch. Furthermore, its light weight (approximately 60 g/m^2) makes possible the deployment of truly large areas from a single Shuttle payload.

The interface between the mesh and the supporting structure depends, of course, not only on the characteristics of the structure itself but, more

importantly, also on the compliance of the mesh. If the mesh has high stiffness against straining tangential to the surface, the interface must be carefully designed to absorb any geometrical differences between the mesh and its supporting structure. If, on the other hand, the mesh is highly compliant, then the mesh can be attached directly to the structure. The relative simplicity of the latter approach, together with the current availability (and flight use) of a gold-plated molybdenum knitted-mesh material, leads to its selection for the present report.

Two deep-truss structural concepts suitable for use with a mesh reflector are illustrated in Figures 8 and 9. The first is a modified version of the variously named "Maypole," "Hoop-and-Column," and "Spoked-Wheel" concepts. The basic structural element is the bicycle-wheel structure made up of the central column (hub) and the compression rim tied together by stays. The rim is articulated, allowing stowage. The central column could be an Astromast. The rest of the structure is "soft" in the sense that its elements need to carry tension only. Thus, a variety of packaging techniques can be used without requiring complex joints. The tension-carrying elements are pretensioned sufficiently to allow incremental compression loading in orbit while still retaining positive tension. The front and back stays, for example, thus maintain their full axial stiffness.

The reflector surface is formed by structural tension-stiffened radial-rib beams. The tension forces in the curved chords automatically pretension the interchord members. The chord pretension is reacted by the compression rim. A compression spreader is needed at the outer end of the radial beam. The pretensioned rib beam is cantilevered at the central hub and also supported at the tip by the rim. Circumferential tension members provide the remainder of the structure. They and the upper chords of the beams are laced through the mesh to provide the necessary shaping to the reflector surface in quadrilateral facets.

The second concept, Figure 9, is the familiar tetrahedral truss treated by many authors. Differences exist in scale and in the manner in which the structure and mesh interface. In the form treated herein, the mesh is fastened only along the surface truss members; no shaping chords or drawing lines are used to shape the mesh surface within each facet. Properly located joints allow stowage and deployment of the otherwise uncompliant structure.

From an overall standpoint, the tetrahedral truss structure can be thought of as a thick shell, the surfaces of which are defined by the lattice nodes. For the equilateral triangular geometry, the equivalent shell is isotropic, an advantage that does not obtain for some of the other truss geometries proposed.

The geodesic dome can be viewed as the limiting case of a tetrahedral truss as the thickness H is reduced to zero. The geodesic dome behaves in the large as a membrane. It is simpler than the truss since only one surface of lattice elements is required. On the other hand, the membrane-like surface is very flexible unless the edge is supported by a stiff ring. Packaging and deploying the ring may present more difficulties than those presented by the more nearly uniform tetrahedral truss.

On either of these concepts, the dominant loading is provided by the tension in the mesh itself. The tension must be sensible and reasonably uniform and isotropic in order to assure good electrical conductivity (and, hence, rf reflectivity) of the mesh. Values of around 2.5 N/m are used, for example, in the Harris studies in Reference 4. A study was reported in Reference 5 which showed that the strength of the structure designed to cope with such a value of mesh tension without intolerable loss of surface accuracy or structural efficiency is sufficient to withstand lateral accelerations many orders of magnitude greater than those expected in orbital operations. In the pretensioned truss, Figure 8, the tension chord members must be pretensioned sufficiently to keep them from bowing excessively due to the inward-directed line loads occurring where the mesh changes direction. These tensions, in turn, must be reacted by the compressive rim and central column. In the tetrahedral truss, the individual struts must be stiff enough to preclude excessive bending due to the same loading. Incidentally, an alternate method of mesh attachment, involving highly pretensioned tendons reeved through the mesh and fastened to the corners of the truss, yielded equivalent truss-strut design requirements.

Selection of Concept for Further Study

The structural concepts appropriate for solid reflector panels show a great deal of attractiveness for precision antennas. They are not suitable for truly large apertures unless multiple Shuttle launches and assembly of

major components in space are allowable. For this reason, attention is concentrated on those concepts utilizing mesh for the reflector.

The pretensioned-truss concept apparently promises the highest degree of packaging efficiency and perhaps the lightest weight. However, it is difficult to conceive of a method for sequentially deploying the structure. While the deployment process may be considered to be simple enough to be able to achieve adequate reliability with synchronous deployment, difficulties in demonstrating the reliability with ground test are paramount.

The tetrahedral truss is the concept of choice. It offers the possibility of a reasonably large aperture with a single Shuttle payload. The difficulty is that the versions reported in the past do not follow the principle of sequential erection. For example, the PETA concept (ref. 6) utilizes a synchronous deployment. Even the two-stage deployment approach of Reference 7 involves the management of large quantities of partially deployed material at stages during the deployment and is, hence, not a sequential deployment.

One of the major contributions of the present paper is the description of a new deployment concept for the sequential erection of tetrahedral truss structures. In addition, the stand-alone stiffness of a truss composed of stiff members allows considerable advantages in ground test. The tetrahedral truss is also more modular in nature allowing the provision of various overall antenna configurations from a single concept. Advances in knowledge can be applied more generally. For example, not only can centrally fed antennas be treated, but also can off-axis feeds be accommodated by mounting the feed structure on the edge of the reflector; no blockage of the rf energy occurs.

An example configuration for a 200-m-diameter antenna is shown in Figure 10. It would meet accuracy requirements of L-band (20-cm wavelength). Some characteristics are shown in the figure. The reflector has about 1000 facets; the next section deals with the new approach to deploying it.

A NEW APPROACH TO THE DEPLOYMENT OF TETRAHEDRAL TRUSSES

The foregoing discussion indicates that the tetrahedral truss structure (or other similar deep-truss configurations) shows great potential for

supporting mesh-type reflecting surfaces. The deployment of such a structure with its mesh attached is an attractive approach to large space antenna reflectors. By its nature, however, the truss involves many thousands of joints, all of which must operate successfully in order to achieve erection of the entire structure. Reliability considerations, therefore, dictate that sequential deployment be employed. Cost considerations dictate that the deployment be automated.

The deployment is envisioned as being actuated and controlled by means of appropriately designed mechanisms mounted on the deployment canisters which also serve to contain and protect the stowed reflector during launch. The structure itself is assumed to be modular and passive, and its joints are required to be as simple as possible in order to reduce cost. Concentrating the complex mechanical devices in the deployment canisters allows external on-off control at all stages of deployment in addition to being cost effective. Incidentally, the complexity of those devices will probably be much less than that of machinery designed for textile and agricultural operations. Also, this approach to deployment is a logical extension of practices presently used for actual spaceflight hardware.

Deployment Schematic

Sequential deployment is easy to achieve schematically for linear structures such as Astromast or STEM booms. On the one side is the packaged boom, on the other is the fully deployed boom, and in the middle is the transition section in which the material is undergoing deployment. The means of achievement are not at all apparent for two-dimensional structures such as the tetrahedral truss, in which the problem is to expand from a small package to a large surface while maintaining the connectivity of the elements.

An approach to sequential deployment of surfaces is illustrated in Figure 11 which shows schematically steps in the deployment from the fully packaged state (a) to fully deployed state (f). The structural truss is articulated in such a way as to allow the generic module to deploy in two stages, first outward from the canister (vertical in the figure) and then in the orthogonal (horizontal) direction. The fully deployed truss portions are held and moved by appropriate actuators mounted to the canister halves. The modules that

have undergone first-stage deployment have good structural integrity in the vertical direction in the figure but very little in the horizontal direction. The full-strength fully deployed segments are therefore used to control the partially deployed structure in its weak direction.

These ideas are illustrated in the figure. Note that the region of partially deployed structure is short and wide during the early steps and becomes longer as the canister halves move themselves apart and thinner as the partially deployed material goes through full deployment. Note also that as each layer of partially deployed material becomes fully deployed, there is a danger of losing full control inasmuch as the full-strength segments cannot remain in intimate contact with the layers underneath. This latter possibility is evident, for example, for the kind of approach used in Reference 7. The approach discussed in the next section avoids the danger.

Sequentially Deployed Tetrahedral Truss

A perspective sketch of the tetrahedral truss is shown in Figure 12 which shows the various hinge joints oversized for clarity. An attempt is made here to convey an idea of the slenderness of the struts in some of the stouter designs. Most projected trusses have much slenderer members.

The nomenclature used for the individual truss members is shown in Figure 13. Note that the truss is considered to be composed of a number of parallel truss "ribs" connected to each other by interrib surface struts and core members as shown. The ribs, of course, would lie in the vertical direction in the schematic diagrams in Figure 11. The first stage of deployment is then to allow the hinges in the center of the upper and lower rib chords to straighten, thereby deploying the ribs one cell at a time. Note that the rib diagonals remain straight at all times; each pair is separated when the chord member straightens.

Figure 14 shows five deployed ribs awaiting second-stage deployment. The pack of ribs is bounded by fully deployed structure on either side. Note that the close packaging of the elements demands that stringent requirements on the length of various members (such as the rib diagonals and the interrib core member) be obeyed. The usual tetrahedral truss geometry does satisfy these requirements.

The second stage of deployment involves the translation of one rib outward from its neighbor, which remains in the pack. The rib moves nominally as a rigid body, being part of the fully deployed truss. The motion is a shearing one, as well as outward, as shown in the single-module sequence in Figure 15. Note that only one pair of interrib surface struts is straightened during second-stage deployment. The other pair has already been straightened during first-stage deployment, being packaged parallel to a chord member.

In order to avoid large overall translations in the rib direction during reflector deployment, the direction of shearing of adjacent ribs is alternated from bay to bay. Thus, every other rib is the same, and the intermediate ones are mirror images. The interrib struts that are active during second-stage deployment form a zig-zag pattern on the surface.

The new approach to deployment is difficult to comprehend although it is actually straightforward. Because of this difficulty, two models have been constructed. They are described in a later section of this report.

Joint Design

Although the sequential-deployment approach is theoretically sound, its practical implementation depends importantly on the availability of inexpensive, simple, reliable, articulating joints which can be operated repeatably with low actuation torque and with very small free-play. A joint which meets these requirements is the simple door hinge. The hinge pin is small, hence even high friction forces yield low torques. The pins can be fitted with very low free-play by ordinary machining methods. By making the width of the hinge as large as possible, the influence of moment components perpendicular to the hinge line can be minimized.

The simple hinge allows only limited joint freedom. For this reason, most designers resort to ball joints or gimbals if other-than-rectilinear motions are encountered. Unfortunately, such joints tend to be complicated and expensive to make accurately enough.

Actually, a simple hinge is capable of producing an arbitrary change in orientation during its rotation. That is the case which can be seen from the following analysis.

Let $\hat{e}_1$ and $\hat{e}_2$ be two unit-vector directions before deployment in a body mounted on the hinge. Let the final orientation after hinge rotation of these two vectors be denoted by $\hat{e}_1'$ and $\hat{e}_2'$. Then the hinge line that will produce this final orientation lies in the direction parallel to

$$\vec{h} = \left(\hat{e}_1 - \hat{e}_2'\right) \times \left(\hat{e}_2 - \hat{e}_2'\right) \tag{1}$$

Inspection shows that this hinge direction does maintain constancy of angle with each of the directions (and, hence, with any direction) in the hinged body. This follows from the fact that any direction perpendicular to the difference of two equal-length vectors has equal angles with the two vectors. The cross product reveals the unique direction which satisfies the angle equality for both vector pairs.

Therefore, a hinge direction can be selected that will produce an arbitrary change in orientation. Of course, the intermediate motion of the hinged body between the two extremes is strictly constrained; misalignments and mislocations can therefore be expected during the process of deployment. In the present situation, the members attached to the hinges are expected to be very slender and, hence, will tolerate a reasonable amount of misfit. The important fact is that the fit is correct and the members are strain-free when packaged and when deployed.

Once the direction of the hinge is found, its location must be determined. Insofar as possible, the hinge line should pass through the centerline of the hinged member. In this way the axial forces can be transmitted through the hinge without causing local bending moments. Since each joint of the truss, of course, is designed in such a way that the member centerlines all pass through the same point (so that all forces stay properly aligned), the only way of achieving this for all members would be to place all the hinges at the joint apex - a mechanical impossibility. Therefore, the joint itself must consist of a "hinge body" to which appropriate members are attached with hinges at their centerlines.

Because of the two-stage deployment sequence, some of the members are hinged to other members rather than to the hinge body. In particular, the

interrib core member during first-stage deployment remains fixed with respect to a rib diagonal; it is accordingly hinged from that diagonal. Similarly, the interrib strut that straightens during first-stage deployment does so along with a rib chord. They are consequently hinged together.

Two members cannot be hinged together with a hinge located at their centerlines; they would interfere with each other when packaged. In this case a departure from the centerline location is necessary. Similarly, the "knee" hinge in the middle of each strut that folds cannot be located at the centerline. In the latter case, the tightest package is obtained by locating the hinge line (whose direction, of course, must be perpendicular to the member axis) at the edge of the strut. This location is used for the models discussed in a later section. It is also used for those two cases in which two members are hinged together.

Whenever hinges are located off the centerline, the hinge joint must be designed carefully so that axial loads can be transmitted through the hinge without causing local bending of the slender members. This is accomplished by preloaded buttresses on the side of the member opposite to the hinge which are pressed together upon full deployment. The amount of preload is set at a comfortable multiple of the expected flight loads so that contact of the buttresses is assured.

For the knee hinges, the preload is supplied by springs in the hinge. Moment amplification can be achieved, if necessary, by appropriately designed levers. Over-center latches should be avoided because of their complexity and their sensitivity to fabrication tolerances. For those members hinged together, adequate preload can usually be obtained by setting the joint geometry so that the buttresses contact slightly before full deployment is achieved.

The hinge body itself is a free body which must be properly oriented. The possibility exists for static instability involving hinge body rotation when the struts are in compression. Care must be taken to assure that no instability will occur. Buttresses may be necessary to assure good control of the hinge-body orientation.

The position of the hinge along the length of the member is selected in such a way as to achieve the best packaging. Insofar as possible, the members

should be tightly packed. In this way the hinge body is also made as compact as possible, reducing the tendency toward instability.

For the present design, the intention is to achieve a high diametral packaging ratio. The motivation is that the Shuttle payload volume is more restricted in its diameter than along its length. Thus, the surface struts and chords are folded outwards. The six surface members intersecting at a joint are packaged as shown in Figure 16. Also shown in the figure is the flat-truss packaging ratio which is smaller perpendicular to the ribs than parallel to them. This means that a circular aperture will have an oval package with the largest dimension in the rib direction.

The implementation of the various joint-design requirements and approaches is shown by the models described in a later section.

Example Hinge Geometry

The determination of the precise hinge-line orientation and location can be performed by inspection for most of the members. However, the interrib surface strut that straightens during second-stage deployment requires special attention. This strut, termed herein the "A" member, connects adjacent ribs and must accommodate the relative shearing motion as well as straightening. In Figure 17 the two A members are shown intersecting at a joint in solid lines. Also shown in dotted lines is the other possible pair of A members. Two Cartesian coordinate systems are used: the (x,y,z) system is based on the surface of the truss; the (ξ,η,ζ) system is based on the rib plane which lies at the angle ψ with respect to the z axis. This angle is related to the ratio of cell size ℓ to truss depth H by

$$\tan \psi = \frac{\ell}{2H} \tan \Lambda \tag{2}$$

where Λ is the "sweep angle" of the A member. Of course, for the standard tetrahedral-truss geometry treated herein, the angle Λ is equal to 30 degrees. Other geometries exist which satisfy the length-equality requirements for sequential packaging referred to in a preceding section. There exists, therefore, a generalized tetrahedral-truss geometry which may be useful.

Also shown in Figure 17 is the knee-hinge orientation for the A member. Note that it is taken to be rotated an angle β in the right-hand sense from the x-y plane. This angle is open to choice by the designer. A good choice would be one that results in a tolerable amount of mismatch during deployment. An investigation was made of the deployment kinematics for an infinitely deep truss ($\psi = 0$) which yielded minimum mismatch for $\beta = 0$. For nonzero ψ, the appropriate value of β is probably also nonzero. For the present design, the β is selected so that the deployed knee hinge line is perpendicular to the packaged member centerline.

For the procedure described by Eq. (1), let $\hat{e}_1$ be the unit vector along the A member centerline and $\hat{e}_2$ be the unit vector along the knee hinge line. Then, in general, components (denoted in matrix form) of the unit vectors in the ξ,η,ζ coordinate system are

$$\hat{e}_1 = \begin{vmatrix} 0 \\ 0 \\ 1 \end{vmatrix} \quad ; \quad \hat{e}_1' = \begin{vmatrix} \sin \Lambda \\ \cos \Lambda \cos \psi \\ -\cos \Lambda \sin \psi \end{vmatrix} \tag{3a}$$

$$\hat{e}_2 = \begin{vmatrix} 1 \\ 0 \\ 0 \end{vmatrix} \quad ; \quad \hat{e}_2' = \begin{vmatrix} \cos \beta \cos \Lambda \\ -\cos \beta \sin \Lambda \cos \psi - \sin \beta \sin \psi \\ \cos \beta \sin \Lambda \sin \psi - \sin \beta \cos \psi \end{vmatrix} \tag{3b}$$

Note that the A member is arbitrarily assumed to stow parallel to the ζ axis. Certainly, the stowage orientation should lie in the rib plane so that all packaged members are parallel. But the direction within the rib plane could be taken to be, for instance, along a rib diagonal. The present choice is made primarily for simplicity. The stowed knee hinge orientation is selected to lie in the rib plane so that the two A members stow side-by-side.

Requiring that the deployed knee hinge line be perpendicular to the stowed centerline yields

$$\tan \beta = \sin \Lambda \tan \psi \tag{4}$$

Using this value for β and applying Eq. (1) yields the desired hinge line direction for the A member

$$\vec{h}_{A_I} = \begin{vmatrix} -\cos \beta \sin \Lambda \, (1 + \cos \Lambda \sin \psi) \\ \cos \psi \, (1 - \cos \beta \cos \Lambda)(1 + \cos \Lambda \sin \psi) \\ \cos \Lambda \cos^2 \psi - \cos \beta \, (1 - \cos^2 \Lambda \sin^2 \psi) \end{vmatrix} \tag{5}$$

By repeating the process for the other three possible A member geometries shown in Figure 17, all of the A hinge lines can be determined. In particular, the hinge orientation for the other solid-line A member in Figure 17 turns out to be

$$\vec{h}_{A_{II}} = \begin{vmatrix} \cos \beta \sin \Lambda \, (1 - \cos \Lambda \sin \psi) \\ \cos \psi \, (1 - \cos \beta \cos \Lambda)(1 - \cos \Lambda \sin \psi) \\ -\cos \Lambda \cos^2 \psi + \cos \beta \, (1 - \cos^2 \Lambda \sin^2 \psi) \end{vmatrix} \tag{6}$$

Note that the ratio of the η component to the ξ component has the same absolute value in all four cases. There exists a fortuitous symmetry of the A hinge lines when viewed parallel to the ζ axis; this simplifies the hardware design and fabrication. The orientations for the dotted-line A members are found by symmetry.

The locations of the hinge lines are found by assuming that the pair of A members stow with their edges at the rib plane. Thus, the stowed centerline must have an η component of d/2 where d is the strut diameter. The hinge line therefore passes through the member-centerline point

$$\vec{P}_{A_I} = \frac{d}{2} \begin{vmatrix} \cos \psi \tan \Lambda \\ 1 \\ -\tan \psi \end{vmatrix} \tag{7}$$

for the right-hand solid A member in Figure 17. The locations of the other three hinge lines are found by symmetry.

DESIGN AND FABRICATION OF MODELS

During development of the tetrahedral truss, two model types have been constructed. One is for visualization of the concept and is thus in form amenable to change and adjustment. The other model type is of high fidelity, demonstrating the concept in operational form. This two-model approach has proven to be successful for other concepts.

Concept Visualization Model

The concept visualization model serves two useful functions. First, since it is made primarily by the inventor, it serves to verify the concept first-hand. The second function is to show others how the concept works. In particular, such a model is necessary to explain the concept to the designer and others who are the ones who must make it practical.

In the present case, the model consists of hinge bodies, hinges, and connecting members. Hinge bodies are made mostly of wood; metal is used if required for strength or convenience. Hinges are standard, hardware-store variety (in this case, 1 inch in width) screwed to the hinge bodies. Care is taken to mount the hinges correctly in position and orientation, both for concept verification and for indication of partial deployment strain. The connecting members are tubular aluminum bonded to the hinge bodies using a rapid-setting epoxy.

Figure 18 shows a cluster of hinges at the center of the upper surface of the model. The main hinge body is aluminum; six wood strut ends hinge directly to it and three hinge indirectly. The tubular aluminum members are bonded into holes in the wood pieces.

Figure 19 shows the deployment of the model. In the first photograph, the model is completely packaged, and in the succeeding four photographs, the ribs undergo first-stage deployment. Lateral shearing of a rib deploys a module (at the end of second page of Figure 19). The third page of Figure 19 shows the second-stage deployment of the other rib.

High Fidelity Model

The second model constructed is the high-fidelity model. The purpose of this model is to approximate more closely the characteristics of an operational structure in terms of slenderness, kinematics of deployment, materials, and, most importantly, joint design.

Engineering and Design

Development of the high-fidelity model made use of the purely numerical results of the hinge position/orientation analysis, as well as the tangible, practical aspects of the concept visualization model. Whereas in the first model only ordinary care was taken to locate the hinges correctly, thus resulting in a reasonable approximation of the theoretical geometry, in the second model the hinges are placed and oriented precisely using sensitive milling machine controls and micrometer measurements. The result is a much greater degree of precision and fidelity to the expected operation of eventual full-scale hardware.

There are 21 design items. One is a general locking hinge which is used on all members which package by folding at midlength, thus requiring a hinge which provides an aligning preload in the deployed condition. The other 20 are actually two sets of ten each, one a right-handed set and the other a left-handed set of the same elements. Of the ten items in each set, one is a hinge body, and the remaining nine are the end pieces of the nine rods which come together at a node of the structure.

Locking Hinge - This hinge, shown in Figure 20, is virtually a locking one due to its almost-over-center latch configuration and has the following properties:

- Because of the geometry of its various linking members, it provides high alignment forces in the deployed configuration.
- It packages so that it takes up the same projected space as the folded member that it hinges.
- The two major pieces into which the rods are bonded are identical.

Nine-Member Joint Cluster - This cluster, shown in Figure 21, is the right-handed version at the central node of the upper (hexagonal) surface of the high-fidelity model.

Members 1 through 6 are in the surface. During packaging, Members 1 and 2 rotate up out of the plane as Members 3 and 4 rotate over to lie adjacent to Member 6. Packaging is completed as Member 5 rotates up, and Members 3, 4, and 6 rotate up as a unit thus resulting in these first six members packaging parallel and adjacent to each other.

Members 7 and 8 are the rib diagonal members. The interrib core Member 9 rotates over to lie adjacent to Member 8 in the same motion as described in the first part of the above paragraph. Then Members 7, 8, and 9 package together as a unit so that in the fully packaged configuration all nine members are parallel.

In the deployed configuration, Members 7 and 8 bear against Item 10, the hinge body. This fixes its orientation. Members 1, 2, 5, and 6 hinge to the body on their centerlines and do not bear against the hinge body. Members 3, 4, and 9 hinge off their centerlines and require bearing surfaces against the hinge body to fix their deployed orientation. These bearing surfaces are precisely located to ensure correct member orientation.

Materials

The materials used in the construction of the high-fidelity model were as follows. Aluminum alloy 2024-T351 was used in the main joint body, the ends of the members, and the locking knee hinges. The members are graphite/epoxy rod of 0.125-inch diameter and various lengths so that the deployed cell size is 12 inches (side of surface equilateral triangle), and the deployed truss depth is also 12 inches. The graphite/epoxy members are bonded to the aluminum ends using Devcon, a two-part, rapidly setting epoxy. Hinge pins are 0.040-inch-diameter drill rod. Stainless steel compression springs are used in the locking hinges.

As delivered, the graphite rods were slightly large in diameter and were slightly bowed. The excess-diameter problem was easily solved by centerless grinding from the as-delivered 0.134 inch to the desired 0.125 inch. The amount of bowing, over a 32-inch length, ranged from less than one-tenth diameter to about one-half diameter. The most bowed pieces were used in the surface members of the tetrahedral truss model because bowing of the short lengths involved is acceptable (less than one-tenth diameter for a rod of 13 inches in length).

Fabrication

Fabrication of aluminum parts was done on milling machines. Special tooling was made where necessary to ensure precise positions and angles of surfaces and holes.

Machining tolerances were made small, typically 0.001 inch, in order that the nominally small parts of typical dimension 0.200 inch were made accurately. Problems were encountered in surfaces making compound angles to the mill axes in that proper ordering of the rotations is essential.

Assembly

Prior to assembly, all hinge clusters and locking hinges were assembled and adjusted where necessary for unrestricted motion. Right- and left-handed clusters were identified. Graphite/epoxy rods were cut to proper length.

All surface members have a locking hinge. Each was bonded as an assembly consisting of a locking hinge and two rods having precise centerline alignment in the deployed condition. Then, referring to Figure 21, the ends of Members 3, 4, 5, and 6 were bonded in place so that the 12-inch nodal distance was obtained and so that precise adjacent packaging is assured. The surface was completed with the bonding of Members 1 and 2 using calculated packaged dimensions which result in an unstrained deployed surface of equilateral triangles. The upper and lower surfaces were assembled in this manner.

Core Members 7, 8, and 9 were bonded in place in the completely packaged configuration using calculated packaged dimensions. Special care was taken to make sure the core members had the proper end pieces required for deployment.

Figures 22 and 23 show various views of the hinges and of the stages of deployment.

Transition Forces

During first-stage deployment, all motion is in the rib plane using hinges perpendicular to the rib plane, and no structural strain occurs during the transition. During second-stage deployment, however, motions are not confined to a plane, and strains occur particularly in the obliquely packaging

surface member. In the model, the restraint due to transition straining can be felt; it is small in terms of allowable levels and is easily overcome, but is clearly evident.

Weights

The model weight, including aluminum joints, was 0.245 kg. The joints weighed 0.135 kg so that the joint factor is $k = m_{total}/m_{rods} = 2.22$. These measurements have meaning only when scaled to full size.

The large reflector shown in Figure 10 has 7-m surface members and a 7-m depth. Graphite/epoxy tubular members have a 40-mm diameter and an assumed 0.35-mm wall thickness. Areal density for the graphite/epoxy members alone is 0.106 kg/m^2.

The areal density due to the joints is determined as follows. A surface triangle of area $\sqrt{3}/4\ell^2$ contains 1/2 joint cluster and 3/2 midhinge. Joint number density is, including upper and lower surfaces, $4/\sqrt{3}\ell^2$ for the clusters and $12/\sqrt{3}\ell^2$ for the knee hinges. In the model, the cluster weight was 0.0080 kg, and the midhinge weight was 0.0017 kg. Scaling for titanium density and for joint size (5.08 mm in model to 40 mm for full scale) yields cluster and knee-hinge weights of 6.6 kg and 1.4 kg. Titanium joint density in the large truss, scaled up from the model, would then be 0.51 kg/m^2.

This anticipated joint density is clearly higher than desired. A reduction of a factor of ten is needed. The joint masses can be predicted by investigating a hypothetical joint cluster consisting of nine short titanium tubes on which to attach the tubular members and sufficient remaining material to connect them. The nine tubes, 0.04-m diameter by 0.001-m wall by 0.08-m length, have a volume 0.00090 m^3, or weight 0.41 kg. The connecting body can be assumed to have weight equal to the tubes; thus, the cluster would weigh 0.82 kg. The corresponding knee hinge would weigh 0.17 kg. This approach yields a theoretical titanium-joint areal density of 0.063 kg/m^2, for a joint k factor of 1.60.

DESIGN OF DOUBLY CURVED REFLECTORS

The preceding development applies strictly to a tetrahedral truss with a flat surface. In fact, most antenna reflectors have a dish-shaped, doubly

curved surface. Inasmuch as the approach followed herein is to mount the reflecting mesh close to the truss structure, some means must be found to make the truss surface doubly curved.

The effects of the curvature over the area of one module of the truss are small. Therefore, the methods for joint design developed for a flat truss can be applied to the curved one with small corrections. On the other hand, reliability of deployment requires that each rib nests with its neighbors. This means that the upper and lower chords and diagonals of adjacent ribs have the same lengths. In addition, in order that the ribs that have undergone first-stage deployment are properly held by the fully deployed truss segments, the ribs on the inner edges of the segments must have nearly the same shape. Finally, the packaged core should be of equal height so that the deployment canister and actuators can be designed to interface with joints at the same elevation throughout the rib. Thus, all ribs should have the same planform and shape, and have constant length diagonals. Furthermore, the interrib members that remain straight during second-stage deployment must have the same length as the rib members that they are stowed against.

The fact is that the sequential deployment concept explained in this report places extremely stringent requirements on the geometry of the truss members. The requirements are so severe that there is apparently no way to meet them for an arbitrarily shaped surface. Fortunately, small amounts of mismatch can be accommodated by modifying the locations of the hinge lines at each joint so that the deployed lengths are changed while keeping packaged lengths the same; the cost is an increase in package size because the joints become less compact.

Most reflectors are paraboloidal in shape. Some are axisymmetric; the ones with off-axis feed are a segment cut from one side of a larger parent paraboloid. In most cases, the dish is fairly shallow, with focal length usually greater than the aperture size. Such a shallow dish can be approximated by a sphere with a radius of about twice the focal length. A sphere, then, is a reasonable shape to start with in attempting to achieve doubly curved surfaces.

The sphere has the advantage that once a design is obtained for a meridional slice, it can be replicated around the sphere enough times to produce the entire surface; thus, attention can be concentrated on only a rib

and its immediate neighbors. Once a spherical design is obtained, then small local changes can be made to achieve the desired paraboloidal shape.

The next section contains a detailed analysis that leads up to the design for a spherical shape. Actually, the shape turns out to be a near sphere - the departure being necessary to achieve the desired equality of surface member lengths and constancy of rib diagonal lengths. The approach is to force all the (apparently) necessary mismatch into the interrib core members. In fact, the result suprisingly shows that there is no mismatch. The resulting design obeys all the stringent requirements without recourse to local hinge-location modification. The design therefore constitutes an excellent foundation for generating other surfaces.

The analysis is valid for the generalized tetrahedral truss, discussed in a preceding section, which includes the equilateral triangle standard tetrahedral truss as a special case. This is accomplished by letting the deployment shearing component be freely chosen. Various geometries can thereby be found for the shape of the surface facets.

Geometrical Analysis for Quasi-Sphere

Consider a Cartesian coordinate system (x,y,z) with the origin located approximately at the center of the reflector side of the truss surface. Let x and y lie tangent to the surface and z be perpendicular to the two in the right-hand sense. The z axis passes through the center of the approximating sphere of radius R, which is, of course, equal to about twice the focal length F.

Consider also the spherical coordinate system (r, θ, ϕ) with origin at the center of the approximating sphere. Let the two coordinate systems be related by

$$\begin{aligned} x &= r \sin \theta \\ y &= r \cos \theta \sin \phi \\ z &= R - r \cos \theta \cos \phi \end{aligned} \tag{8}$$

The central rib and its two neighbors are shown in Figure 24. Also shown are the interrib members that remain straight during the second stage of deployment. The A members are omitted for clarity. Note that the interrib core members are shown dotted.

The numbering system shown is useful for identifying the joints in the ribs. The upper-chord joints are designated by odd numbers and the lower-chord joints by even numbers, with n = 0 being at the center of the rib. The joints on adjacent ribs are numbered in such a way that similarly numbered joints merge on stowage.

Recall that the objective is to ensure that all ribs have the same geometry and can be matched by a rigid-body motion. Thus, the location of the joints in any rib can be determined if the geometry of the central rib is known and if the rigid-body motion is specified. Consider all the ribs to be packaged together. Let the spherical coordinates prior to rigid-body motion of the central-rib joint n be given by (r_n, θ_n, ϕ_n). Then let the central rib be rotated by the angle $\gamma/2$ in the positive θ direction about an axis passing through the sphere center and parallel to the y axis. Similarly, let the left- and right-hand ribs be rotated by the angle $\gamma/2$ in the negative θ direction about the same axis and then outward by the angle δ in the negative and positive ϕ directions about the axis passing through the sphere center and parallel to the rotated x axis. The resulting Cartesian coordinates of the nth joint for the central would then be

$$\begin{vmatrix} x \\ y \\ R-z \end{vmatrix}_n = r_n \begin{vmatrix} \cos\frac{\gamma}{2}\sin\phi_n + \sin\frac{\gamma}{2}\cos\theta_n\cos\phi_n \\ \cos\theta_n\sin\phi_n \\ -\sin\frac{\gamma}{2}\sin\theta_n + \cos\frac{\gamma}{2}\cos\theta_n\cos\phi_n \end{vmatrix} \tag{9a}$$

and for the adjacent ribs

$$\begin{vmatrix} x \\ y \\ R-z \end{vmatrix}_n = r_n \begin{vmatrix} \cos\frac{\gamma}{2}\sin\theta_n - \sin\frac{\gamma}{2}\cos\theta_n\cos\phi_n \\ \cos\delta\cos\theta_n\sin\phi_n + \sin\delta\left(\sin\frac{\gamma}{2}\sin\theta_n + \cos\frac{\gamma}{2}\cos\theta_n\cos\phi_n\right) \\ + \sin\delta\cos\theta_n\sin\phi_n + \cos\delta\left(\sin\frac{\gamma}{2}\sin\theta_n + \cos\frac{\gamma}{2}\cos\theta_n\cos\phi_n\right) \end{vmatrix} \tag{9b}$$

where the upper sign pertains to the right-hand rib and the lower sign to the left-hand rib.

The value of r_n, θ_n, and ϕ_n should be chosen so that the lengths of the various members that must package together are the same. In fact, however, this requirement appears to be unachievable. Examination of the numbers of constraints and degrees of freedom indicates that there should exist mismatch in the lengths of one member pair for each bay along the rib. This mismatch could be accommodated by moving the hinge lines of the mismatched members so that they can have different deployed and packaged effective lengths. Of course, the selection of the particular member to be used to absorb the mismatch is somewhat arbitrary; in the present analysis, the mismatch is accommodated in the interrib core members (which are shown dotted in Figure 24).

Equality of lengths of surface-member pairs is accomplished as follows. Consider the points n and n-2 on center rib and the point n on each adjacent rib. The three lines shown in Figure 24 connecting these four points must all be the same length. Satisfying the length equality yields two equations which can be manipulated to give

$$\tan\phi_n \tan\phi_{n-2} - \frac{1}{\chi_n^2 \cos^2\frac{\delta}{2}\cos^2\frac{\gamma}{2} - \sin^2\frac{\delta}{2}} \tag{10}$$

$$\chi_n = \frac{\cos\phi_n + \tan\frac{\gamma}{2}\tan\theta_n}{\sin\phi_n} = \frac{\cos\phi_{n-2} - \tan\frac{\gamma}{2}\tan\theta_{n-2}}{\sin\phi_{n-2}} \tag{11}$$

These two equations can be used to determine the angular coordinates of all the points on either the upper or lower surface providing that a starting point is specified on that surface. Note that the relationships are used recursively with n increasing or decreasing by choosing the appropriate form of χ_n for Eq. (10).

On the center rib, the value of ϕ_n on the upper surface will be found to be zero everywhere. The equations are undefined. Dividing Eq. (10) by sin ϕ_n sin ϕ_{n-2} and taking limits for small ϕ_n yields, for n odd

$$\phi_n = 0 \tag{12}$$

$$\left(1 + \tan \frac{\gamma}{2} \tan \theta_n\right) \left(1 - \tan \frac{\gamma}{2} \theta_{n-2}\right) = \frac{1}{\cos^2 \frac{\delta}{2} \cos^2 \frac{\gamma}{2}} \tag{13}$$

as the appropriate recursion formula.

Note that the radial dimension r_n does not enter into these relations. This is due to the fact that the three equal lengths connect a single point to three points with equal values of r_n. Therefore, the angular coordinates can be defined first, and then the radial dimensions can be found by specifying the length of the rib diagonals.

Let the length of the rib diagonal be d. Then setting the length between points n and n-1 to be d gives the relation

$$r_n^2 + r_{n-1}^2 - 2r_n r_{n-1} \left[\cos \theta_n \cos \theta_{n-1} \cos \left(\phi_n - \phi_{n-1}\right) + \sin \theta_n \sin \theta_{n-1}\right] = d^2 \tag{14}$$

This can be used recursively in either direction to obtain the radial coordinates.

In practice, the most convenient approach is to define the geometry at the center and then to proceed to the rim in both directions, determining angular and radial coordinates of each point along the way. The geometry at the center is given for the upper surface as

$$
\begin{aligned}
r_{+1} &= R \\
\theta_{+1} &= +\frac{\varepsilon_0}{2} \\
\phi_{+1} &= 0
\end{aligned}
\tag{15}
$$

where

$$
\varepsilon_0 = 2 \tan^{-1} \frac{\ell}{2R} \tag{16}
$$

is the angle subtended by the central strut of length ℓ joining points ±1.

Substituting into Eq. (13) for n = 1 yields

$$
\cos \frac{\delta}{2} = \frac{\cos \frac{\varepsilon_0}{2}}{\cos \frac{\varepsilon_0 - \gamma}{2}} \tag{17}
$$

Note that when $\gamma = \varepsilon_0$, the facets are square with the A members being 45-degree diagonals. When $\gamma = \varepsilon_0/2$, the triangles, including the A members, are nominally equilateral.

Symmetry dictates that the center point on the lower surface has a zero value of θ. Its value of ϕ_0 could be considered to be a design variable chosen in order to minimize the maximum disparity between the actual lengths of the interrib core members and the length of the rib diagonal. A good choice for ϕ_0 would appear to be the value for which the interrib core member connecting the point 0 on the center to the point 1 on the right-hand rib has

the correct length. In fact, the numerical calculations in the next section show that this choice is a very good one indeed, inasmuch as all the interrib core members turn out to have exactly the correct length! The expression for ϕ_0 is

$$\phi_0 = \tan^{-1} \frac{1 - \cos\frac{\delta}{2}\cos\frac{\gamma}{2}}{\sin\frac{\delta}{2}} \tag{18}$$

Substituting for n = 0 in Eq. (14) yields

$$r_0 = R\cos\frac{\varepsilon_0}{2}\cos\phi_0 + \sqrt{d^2 - R^2\left(1 - \cos^2\frac{\varepsilon_0}{2}\cos^2\phi_0\right)} \tag{19}$$

Note that the rib-diagonal length can be written in terms of the nominal truss depth $H = (r_0 - R)$ for a shallow curved truss as

$$d = \sqrt{H^2 + \frac{1 - \cos\frac{\varepsilon_0}{2}\cos\phi_0}{2\sin^2\frac{\varepsilon_0}{2}}\,\ell^2} \tag{20}$$

With the points 0 and ±1 so defined, the remaining points can be determined by using Eqs. (10) through (14) recursively as appropriate. The task is simplified because the results are symmetric. That is,

$$\begin{aligned} \theta_{-n} &= -\theta_n \\ \phi_{-n} &= \phi_n \\ r_{-n} &= r_n \end{aligned} \tag{21}$$

Thus, only positive values of n need be considered.

Numerical Examples

The equations developed in the preceding section have been programmed in the interactive FORTRAN computer program which is listed in Table 1. This program compiles and runs on the VAX-11 computer and is particularly suitable for use with a remote terminal. Double-precision calculations are used throughout.

The printout of a sample run is given in Table 2. Note that the user is first asked to specify the value of λ (= γ/ε_0) and then the important reflector design quantities F/D, ℓ/D, and H/ℓ. The program then calculates and displays the values of ε_0, γ, and δ in radians.

The joint geometry is then tabulated for the upper chord in the two left-hand columns and the lower chord in the next two. The first of the pair of columns in each case includes the joint number n and the spherical coordinates. For the upper chord, the value of ϕ_n is omitted. (It is always zero.) The difference between the radial coordinate and the radius to the "tangent" paraboloid at the deployed value of θ (= $\theta_n + \gamma/2$) is given as DELR. The tangent paraboloid coincides with the quasi-sphere at its center and has a focal length of R/2. Note that all lengths are given in terms of the upper-surface chord length at the center.

This difference DELR is a good approximation for the normal displacement between the desired paraboloid and the tangent quasi-sphere. Incidentally, much smaller maximum errors can be achieved by selecting a better-fit quasi-sphere with smaller radius R and centered slightly below the paraboloid.

The second of the pairs of columns gives the Cartesian coordinates (x,y,z) for the rib joint before second-stage deployment. Between adjacent joint tabulations, the length ℓ_n of the rib chord is shown.

The fifth column gives the length of the interrib core member attached to the joint. Note that they are all the same.

The calculations and display are stopped when the x coordinate of the fully deployed rib (on the negative n side) exceeds half the diameter. The

user is then asked for the next design values. The continuation of the session is included in Table 2 which gives the geometries for a reflector with $F/D = 0.5$, 1.0, and 2.0 for $H/\ell = 1$ and 3.

The facet size in the examples shown in Table 2 was selected purposely to be unrealistically coarse so that the influence of various design parameters could be readily shown. A more realistic example is shown in Table 3. Design variables appropriate to the antenna shown in Figure 10 are chosen.

NATURAL VIBRATION OF SHALLOW SHELLS

One of the most important structural characteristics of a space antenna structure is its natural vibration behavior. In Reference 8, the vibration frequency is shown to be the basic quantity for estimating the effects of external disturbance and control accelerations as well as the determination of the degree of interaction between structural flexibility and the control system. In addition, the vibration frequencies are shown in Reference 1 to be the basic information from which the influence of manufacturing errors can be estimated. There is a need therefore to determine, at least approximately, the vibration frequencies of the truss structure even at the present conceptual stage of development. A precise analysis requires precise definition of the structure and is, hence, inappropriate. On the other hand, by modeling the truss structure as a thin shell, results can be obtained that are useful for conceptual and preliminary design.

For flat trusses (which model as plates), the literature (see ref. 9, for example) is replete with useful example analyses that can be used to aid in determining the vibration frequencies of a particular structure. For a doubly curved truss, the situation is unfortunately bleak. Apparently, researchers in the vibration of thin shells tend to include all the possible secondary effects of transverse shear, rotary inertia, and tangential inertia along with the effects of curvature. The analyses are accordingly complicated, and it is difficult to extract the desired information. There is a need, therefore, for a straightforward treatment of a thin-shell problem.

Such a treatment was given by Reissner in Reference 10 for a simply supported rectangular shallow shell. The results are used extensively in Reference 1 but are recognized as being only partly appropriate to the

circular planforms with free edges often encountered in space antennas. The purpose of the present section is to solve Reissner's shallow-shell equations for circular planforms with simply supported and free edges.

Differential Equations

As shown in Reference 10, the governing differential equations of shallow shells can be reduced to two coupled differential equations for the normal displacement w and an Airy stress function Φ. For sinusoidal vibration at frequency ω of a spherical shell of radius 2F, these differential equations are

$$\begin{aligned} \nabla^4\Phi &= -\frac{(Eh)_s}{2F}\nabla^2 w \\ \nabla^4 w &= \frac{m\omega^2}{D_s} w + \frac{1}{2FD_s}\nabla^2\Phi \end{aligned} \tag{22}$$

where the shell bending stiffness is D_s, membrane stiffness is $(Eh)_s$, and areal density is m. The Laplacian and double Laplacian are written as usual.

Boundary Conditions

For a free edge, the edge moment and Kelvin-Kirchoff edge shear must be zero. Also, the midsurface normal and shear stress resultant must be zero at the edge. For a circular planform of radius r = D/2, these can be written in polar (r,θ) coordinates as

$$\left.\begin{aligned} &\frac{\partial^2 w}{\partial r^2} + \nu\left(\frac{1}{r}\frac{\partial w}{\partial r} + \frac{1}{r^2}\frac{\partial^2 w}{\partial\theta^2}\right) = 0 \\ &\frac{\partial}{\partial r}(\nabla^2 w) + \frac{1-\nu}{r}\frac{\partial^2}{\partial r\partial\theta}\left(\frac{1}{r}\frac{\partial w}{\partial\theta}\right) \\ &\frac{1}{r^2}\frac{\partial^2\Phi}{\partial\theta^2} + \frac{1}{r}\frac{\partial\Phi}{\partial r} = 0 \\ &-\frac{1}{r}\frac{\partial^2}{\partial r\partial\theta}\left(\frac{1}{r}\Phi\right) = 0 \end{aligned}\right\} \tag{23}$$

For simple support, the edge is assumed to be restrained against motion normal to the surface and tangential to the edge. In-surface motion is allowed to be free. Thus, the normal midsurface stress resultant is zero. Since the normal stress resultant and the tangential strain are zero at the edge, then so is the tangential stress resultant. Thus, by deduction, at the edge

$$w = 0$$

$$\frac{\partial^2 w}{\partial r^2} + \frac{\nu}{r}\frac{\partial w}{\partial r} = 0$$

$$\frac{1}{r}\frac{\partial \Phi}{\partial r} + \frac{1}{r^2}\frac{\partial^2 \Phi}{\partial \theta^2} = 0$$

$$\nabla^2 \Phi = 0$$

Solutions

The first of Eq. (22) can be integrated to yield

$$\nabla^2 \Phi + \frac{(Eh)_s}{2F} w = \Psi \tag{24}$$

where

$$\nabla^2 \Psi = 0 \tag{25}$$

Substituting into the second of Eq. (22) gives

$$\nabla^4 w = \left[\frac{m\omega^2}{D_s} - \frac{(Eh)_s}{4F^2 D_s}\right] w + \frac{1}{2FD_s}\Psi \tag{26}$$

Consider first the simply supported case. Since both w and $\nabla^2\Phi$ are zero at the edge, then so is Ψ. Therefore, the solution to Eq. (25) is $\Psi = 0$, and Eq. (26) can be rewritten

$$\nabla^4 w = \frac{m\omega_f^2}{D_s} w \tag{27}$$

where the substitution involving ω_f is obvious. The boundary conditions specify that w and the edge moment are zero. Therefore, the problem has been reduced to that of vibration of a flat plate with the same planform as that of the shell with ω_f as the natural frequency. Therefore, the shell frequency can be obtained from the equivalent flat-plate frequency as

$$\omega^2 = \omega_f^2 + \frac{(Eh)_s}{4mF^2} \tag{28}$$

for simply supported edges. Incidentally, examination of the more general case shows that this result obtains for planforms of all shapes.

Consider now the free-edge case. No such simple solution exists, even for a circular planform; the determination of closed-form solutions involves Bessel functions of complex argument.

The analysis is straightforward. As can be expected, the vibration modes are sinusoidal in the circumferential direction. Let n be the number of waves around the circumference. Then the general, nonsingular solution of Eq. (25) is

$$\psi = C_3 r^n \cos n\theta$$

Substituting into Eq. (26) and integrating yields

$$w = \left[C_1 J_n(kr) + C_2 I_n(kr) - \frac{C_3 r^n}{2FDk^4} \right] \cos n\theta$$

where

$$k^4 = \frac{m\omega^2}{D_s} - \frac{(Eh)_s}{4F^2 D_s}$$

Similarly, integrating Eq. (24) gives

$$\phi = \left\{ \frac{(Eh)_s}{2Fk^2} \left[C_1 J_n(kr) - C_2 I_n(kr) \right] + \frac{C_3 r^{n+2}}{4(n+1)} \left[1 + \frac{(Eh)_s}{4F^2 D_s k^4} \right] + C_4 r^n \right\} \cos n\theta$$

These expressions are substituted into the boundary conditions, Eq. (23), to yield four homogenous equations for the coefficients C_1, C_2, C_3, and C_4. Then values of k are sought which yield nontrivial solutions. The calculations are arduous, especially since most of the solutions involve negative values of k^4, therefore entailing the use of Ber and Bei functions.

The calculations were performed by Mr. Paul T. Suyker who obtained the following results. For n = 0 and 1, all the frequencies are given in terms of circular flat-plate free-edge frequencies by Eq. (28) with very good accuracy. For n = 2 and greater, the lowest frequency for each n is only slightly affected by the curvature, and all the rest are given to good accuracy by Eq. (28).

Example results for n = 2 are shown in Figure 25. Here the frequency parameter is plotted against the curvature parameter $D^2/(Fh_{eq})$. The quantity h_{eq} is the thickness of the equivalent shell. It is equal to $\sqrt{3}H$ for the tetrahedral truss. Note that a truss can be geometrically shallow but structurally highly curved if H is small enough. The increase in frequency for all but the lowest frequency is indistinguishable from that given by Eq. (28). For the lowest frequency, the increase is very slight, with a hop occurring at a value of the frequency parameter of about 200. Incidentally, the frequency for the design shown in Figure 10 is obtained from this figure.

The value of the curvature parameter for that design is about 20, well within the flat range. Thus, performance estimates based on an equivalent flat truss should be valid.

For large values of the curvature parameter, the results are dominated by curvature effects. Then frequencies can be estimated from Eq. (28) by setting the equivalent flat-plate frequency equal to zero. For the lowest frequency, the estimate can be obtained by taking the limit in the first of Eq. (22) as F becomes small. Then $\nabla^2 w = 0$, the solution to which is

$$w = Ar^n \cos n\theta \tag{29}$$

Note that for n = 0 or 1, this displacement shape is a rigid-body motion. For higher values of n, the shape represents an inextensional deformation.

The strain energy density for this situation arises only from bending and is

$$\text{S.E.} = \frac{D_s}{2}\left(\nabla^2 w\right)^2 + (1-\nu)D_s\left\{\left[\frac{\partial}{\partial r}\left(\frac{1}{r}\frac{\partial w}{\partial \theta}\right)\right]^2 - \frac{\partial^2 w}{\partial r^2}\left(\frac{1}{r}\frac{\partial w}{\partial r} + \frac{1}{r^2}\frac{\partial^2 w}{\partial \theta^2}\right)\right\} \tag{30}$$

Using the deformation shape given by Eq. (29) to calculate the Rayleigh quotient yields the desired frequency estimation

$$\omega_n \sqrt{\frac{mD^4}{16D_s}} = 2n\sqrt{(1-\nu)(n^2-1)} \tag{31}$$

For n = 2 and ν = 0.33, this gives a value of 5.67 in comparison with the flat-plate value (ref. 9) of 5.25.

CONCLUDING REMARKS

The new sequential deployment concept explained in this report constitutes a major step toward reliable deployment of large precision antenna reflectors in space. It is only the first step, however. Much needs to be done in developing truss hardware that closely resembles a flight configuration. Only then can meaningful structural tests be conducted to demonstrate the truss stiffness and its behavioral characteristics. Also, detailed conceptual and development effort should be devoted to the deployment mechanisms needed to power the reliable deployment. A solid foundation of analysis needs to be established.

The concept can also serve as a basis for structural configurations other than the tetrahedral truss. The generalization to a truss with the same connectivity but different facet shaping is described in this report. Other topologies may be better in some situations. In all cases, however, the concepts should be guided by the principles of sequential erection and careful joint design set forward in the report.

REFERENCES

1. Hedgepeth, John M.: Influence of Fabrication Tolerances on the Surface Accuracy of Large Antenna Structures. AIAA Journal, vol. 20, No. 5, pp. 680-686, May 1982.

2. Hedgepeth, John M.: Accuracy Potentials for Large Space Antenna Reflectors with Passive Structure. J. Spacecraft and Rockets, vol. 19, No. 3, pp. 211-217, May-June 1982.

3. Crawford, Robert F.; and Coyner, John V., Jr.: Design Concepts and Parametric Studies of Large-Area Structures, Final Report. Astro Research Corporation, ARC-R-1008, March 1976.

4. Montgomery, D.C.; and Sikes, L.D.: Development of the Maypole (Hoop/Column) Deployable Reflector Concept for Large Space Systems Applications. Large Space Systems Technology - 1979 Technology Review, Hampton, Virginia. NASA Conference Publication 2118, 7-8 November 1979.

5. Hedgepeth, John M.: Large Space Systems/Low-Thrust Propulsion Laboratory. Presented at An Industry-Government Information Exchange held at NASA Lewis Research Center, Cleveland, Ohio. NASA Conference Publication 2144, 20-21 May 1980.

6. Fager, J.A.: Large Space Erectable Antenna Stiffness Requirements. J. of Spacecraft and Rockets, vol. 17, pp. 86-92, April 1980.

7. Coyner, J.V.; and Tobey, W.H.: Space-Deployable Box Truss Structure Design. Presented at 15th Aerospace Mechanisms Symposium, George C. Marshall Space Flight Center, Alabama, May 1981.

8. Hedgepeth, John M.: Critical Requirements for the Design of Large Space Structures. NASA CR-3484, November 1981.

9. Leissa, A.W.: Vibration of Plates. NASA SP-160, 1969.

10. Reissner, E.: On Transverse Vibration of Thin, Shallow Elastic Shells. Quarterly Appl. Math, vol. 13, no. 2, pp. 169-176, July 1955.

TABLE 1. FORTRAN COMPUTER PROGRAM FOR QUASISPHERE GEOMETRY.

```
QUASISPH.FOR
C    JOINT GEOMETRY OF QUASISPHERICAL TETRATRUSS
C       INTERRIB CORE MEMBER ADJUSTMENT       JMH 14-AUG-82
C
C
C
        IMPLICIT REAL*8(A-H,O-Z)
        REAL*8 K1,K2,L,LOVERD
        PRINT 100
  100   FORMAT(///T17,' JOINT GEOMETRY OF QUASISPHERICAL TETRATRUSS
     .       '///' NOTE:LAMBDA DETERMINES THE "SWEEP RATIO" OF GEOMETRY'
     .        /'      FOR EXAMPLE,LAMBDA=1.0  FOR "SQUARE"'
     .        /'=0.5  FOR "EQUILATERAL"')
C
C
C
C       SET UP PROPORTIONS
C
 200    CONTINUE
        PRINT 25
  25    FORMAT(' SWEEP RATIO,                    LAMBDA = ',$)
        ACCEPT *,CO
        PRINT 1
  1     FORMAT(' RATIO OF FOCAL LENGTH TO DIAMETER, F/D= '$)
        ACCEPT *,F
        PRINT 2
  2     FORMAT(' RATIO OF MEMBER LENGTH TO DIAMETER,L/D= ',$)
        ACCEPT *,LOVERD
        PRINT 3
  3     FORMAT(' H/L,                                H= ',$)
        ACCEPT *,H
        R=2.*F/LOVERD
        EPS=2.*ASIN(.5/R)
        RADIUS=.5/LOVERD
        GAM=2.*ATAN(CO*TAN(EPS/2.))
        DEL=2.*ACOS(COS(EPS/2.)/COS(EPS/2.-GAM/2.))
  4     FORMAT('  EPSILON=',F10.6,'  GAMMA=',F10.6,'  DELTA=',F10.6)
        C1=COS(DEL)
        C2=COS(DEL/2.)*COS(GAM/2.)
        C3=TAN(GAM/2.)
        C4=SIN(DEL)
        C5=COS(GAM/2.)
        PHI=ATAN((1.-C2)/SIN(DEL/2.))
        D=SQRT(H*H+(1.-COS(EPS/2.)*COS(PHI))/2./(SIN(EPS/2.))**2)
C
C
C       EVALUATE CENTRAL POINTS
C
        SIGN=1
        N=-1
        C4=ABS(C4)
C
        B2=COS(EPS/2.)*COS(PHI)
        THET1=-EPS/2.
        PHI1=0
        R1=R
        XI1=R1*SIN(THET1)
        ET1=0
        ZE1=R1*COS(THET1)
        THET2=0
        PHI2=PHI
        R2=R*(B2+SQRT(D*D/R/R+B2*B2-1.))
        XI2=0
        ET2=R2*SIN(PHI2)
        ZE2=R2*COS(PHI2)
```

TABLE 1. Continued.

```
      THET=EPS/2.
      PHI=0
      R0=R
      XI=-XI1
      ET=0
      ZE=ZE1
      PRINT 4,EPS,GAM,DEL
C
C     DISPLAY HEADING
C
C
      PRINT 5
  5   FORMAT(//T20,'JOINT COORDINATES (TRIADS) AND STRUT LENGTHS'
     . /T20,'FOR STANDARD RIB BEFORE SECOND-STAGE DEPLOYMENT'//
     . T10,'UPPER CHORD',T39,'LOWER CHORD',T65,'CORE MEMBER'/)
C
C     CALCULATE MEMBER LENGTHS
C
 300  D1=SQRT((XI-XI1)**2+(ET-ET1)**2+(ZE-ZE1)**2)
      D2=SQRT(C5*C5*(XI-XI2-C3*(ZE+ZE2))**2+(C1*ET-ET2+C4*C5
     . *(C3*XI+ZE))**2+(C5*C3*(C1*XI+XI2)+C5*(C1*ZE-ZE2)-C4*ET)**2)
      C4=-C4
      N=N+1
C
C     PRINT LOWER-CHORD COORDINATES
C
      PRINT 51,N
      PRINT 61,THET2,XI2,D2
      PRINT 71,D1,PHI2,ET2
      PRINT 81,R2,R-ZE2
C
      THET1=THET2
      PHI1=PHI2
      R1=R2
      XI1=XI2
      ET1=ET2
      ZE1=ZE2
      THET2=THET
      PHI2=PHI
      R2=R0
      XI2=XI
      ET2=ET
      ZE2=ZE
C
C     CALCULATE NEXT LOWER-CHORD POINT
C
      CHI=(COS(PHI1)-C3*TAN(THET1))/SIN(PHI1)
      PHI=ATAN(1./TAN(PHI1)/(C2*C2*CHI*CHI-.5+.5*C1))
      THET=ATAN((SIN(PHI)*CHI-COS(PHI))/C3)
      B2=COS(THET)*COS(THET2)*COS(PHI-PHI2)+SIN(THET)*SIN(THET2)
      R0=B2*R2+SIGN*SQRT(D*D-R2*R2+R2*R2*B2*B2)
      SIGN=-SIGN
      XI=R0*SIN(THET)
      ET=R0*COS(THET)*SIN(PHI)
      ZE=R0*COS(THET)*COS(PHI)
C
C     CALCULATE MEMBER LENGTHS
C
      D1=SQRT((XI-XI1)**2+(ET-ET1)**2+(ZE-ZE1)**2)
      D2=SQRT(C5*C5*(XI-XI2-C3*(ZE+ZE2))**2+(C1*ET-ET2+C4*C5
     . *(C3*XI+ZE))**2+(C5*C3*(C1*XI+XI2)+C5*(C1*ZE-ZE2)-C4*ET)**2)
      C4=-C4
      N=N+1
      C6=COS(THET2+GAM/2.)
      RP=R*(SQRT(2.-C6*C6)-C6)/(1.-C6*C6)
```

TABLE 1. Concluded.

```
C
C       PRINT UPPER-CHORD COORDINATES
C
        PRINT 11,N
        PRINT 21,THET2,XI2,D2
        PRINT 31,R2,ET2,D1
        PRINT 41,RP-R2,R-ZE2
   15   THET1=THET2
        PHI1=PHI2
        R1=R2
        XI1=XI2
        ET1=ET2
        ZE1=ZE2
        THET2=THET
        PHI2=PHI
        R2=R0
        XI2=XI
        ET2=ET
        ZE2=ZE
        IF (R1*SIN(THET1-GAM/2.).GT.RADIUS) GO TO 260
C
C       CALCULATE NEXT UPPER-CHORD POINT
C
        THET=ATAN((-1.+1./C2/C2/(1.-C3*TAN(THET1)))/C3)
        PHI=0
        B2=COS(THET)*COS(THET2)*COS(PHI-PHI2)+SIN(THET)*SIN(THET2)
        R0=B2*R2+SIGN*SQRT(D*D-R2*R2+R2*R2*B2*B2)
        SIGN=-SIGN
        XI=R0*SIN(THET)
        ET=R0*COS(THET)*SIN(PHI)
        ZE=R0*COS(THET)*COS(PHI)
        GO TO 300
  260   CONTINUE
        PRINT 91
  91    FORMAT(/' LOOP BACK ? (NO=0,YES=1)',$)
        ACCEPT *,K1
        IF (K1) 230,230,200
  230   CONTINUE
  11    FORMAT(' N=',I3)
  21    FORMAT(' THETA=',F9.6,T18,F10.6,T63,'LCOR=',F9.6)
  31    FORMAT('    RN=',F10.6,T18,F10.6,T44,'LN=',F10.6)
  41    FORMAT('  DELR=',F10.6,T18,F10.6)
  51    FORMAT(T30,' N=',I3)
  61    FORMAT(T30,' THETA=',F9.6,T47,F10.6,T63,'LCOR=',F9.6)
  71    FORMAT(T15,'LN=',F10.6,T30,'   PHI=',F9.6,T47,F10.6)
  81    FORMAT(T30,'    RN=',F10.6,T47,F10.6)
        END
```

TABLE 2. EXAMPLE INTERACTIVE SESSION.

```
RUN QUASISPH


                JOINT GEOMETRY OF QUASISPHERICAL TETRATRUSS

NOTE:LAMBDA DETERMINES THE "SWEEP RATIO" OF GEOMETRY
     FOR EXAMPLE,LAMBDA=1.0  FOR "SQUARE"
        =0.5  FOR "EQUILATERAL"
SWEEP RATIO,                    LAMBDA = .5
RATIO OF FOCAL LENGTH TO DIAMETER, F/D= .5
RATIO OF MEMBER LENGTH TO DIAMETER,L/D= .2
H/L,                                H= 1
 EPSILON=  0.200335  GAMMA=  0.100419  DELTA=  0.173713


                JOINT COORDINATES (TRIADS) AND STRUT LENGTHS
                FOR STANDARD RIB BEFORE SECOND-STAGE DEPLOYMENT

       UPPER CHORD                LOWER CHORD                CORE MEMBER

                                N=  0
                                THETA= 0.000000   0.000000      LCOR= 1.154942
            LN=  1.000000         PHI= 0.057864   0.345090
                                   RN=  5.967168 -0.957181
N=  1
THETA= 0.100167   0.500000                                      LCOR= 1.154942
   RN=  5.000000  0.000000                LN=  1.185985
 DELR=  0.000315  0.025063
                                N=  2
                                THETA= 0.199013   1.180493      LCOR= 1.154942
            LN=  0.970122         PHI= 0.058450   0.341925
                                   RN=  5.971068 -0.843216
N=  3
THETA= 0.294712   1.448915                                      LCOR= 1.154942
   RN=  4.988269  0.000000                LN=  1.121428
 DELR=  0.019948  0.226797
                                N=  4
                                THETA= 0.386938   2.256744      LCOR= 1.154942
            LN=  0.891249         PHI= 0.060256   0.333515
                                   RN=  5.980426 -0.528234
N=  5
THETA= 0.473907   2.268288                                      LCOR= 1.154942
   RN=  4.970325  0.000000                LN=  1.012872
 DELR=  0.069995  0.577444
                                N=  6
                                THETA= 0.556327   3.163531      LCOR= 1.154942
            LN=  0.787333         PHI= 0.063436   0.322505
                                   RN=  5.990729 -0.077096
N=  7
THETA= 0.632731   2.928329                                      LCOR= 1.154942
   RN=  4.951943  0.000000                LN=  0.887627
 DELR=  0.154788  1.006676
```

TABLE 2. Continued.

```
LOOP BACK ? (NO=0,YES=1)1
SWEEP RATIO,                    LAMBDA = .5
RATIO OF FOCAL LENGTH TO DIAMETER, F/D= 1
RATIO OF MEMBER LENGTH TO DIAMETER,L/D= .2
H/L,                                H= 1
 EPSILON=  0.100042  GAMMA=  0.050052  DELTA=  0.086666

                JOINT COORDINATES (TRIADS) AND STRUT LENGTHS
                FOR STANDARD RIB BEFORE SECOND-STAGE DEPLOYMENT

       UPPER CHORD                  LOWER CHORD                CORE MEMBER

                                N=  0
                                THETA= 0.000000   0.000000      LCOR= 1.154761
            LN=  1.000000         PHI= 0.028884   0.317198
                                   RN= 10.983465 -0.978884
N=  1
THETA= 0.050021   0.500000                                      LCOR= 1.154761
   RN= 10.000000  0.000000                LN=  1.096568
 DELR=  0.000040  0.012508
                                N=  2
                                THETA= 0.099875   1.095246      LCOR= 1.154761
            LN=  0.992443         PHI= 0.028956   0.316434
                                   RN= 10.984376 -0.925055
N=  3
THETA= 0.149319   1.487237                                      LCOR= 1.154761
   RN=  9.997220  0.000000                LN=  1.080623
 DELR=  0.003913  0.114024
                                N=  4
                                THETA= 0.198281   2.164260      LCOR= 1.154761
            LN=  0.970516         PHI= 0.029175   0.314217
                                   RN= 10.986956 -0.767101
N=  5
THETA= 0.246460   2.437782                                      LCOR= 1.154761
   RN=  9.992040  0.000000                LN=  1.050215
 DELR=  0.014439  0.309898
                                N=  6
                                THETA= 0.293887   3.183758      LCOR= 1.154761
            LN=  0.936275         PHI= 0.029544   0.310749
                                   RN= 10.990802 -0.514982
N=  7
THETA= 0.340226   3.332033                                      LCOR= 1.154761
   RN=  9.985102  0.000000                LN=  1.007989
 DELR=  0.035391  0.587253
```

TABLE 2. Continued.

```
LOOP BACK ? (NO=0,YES=1)1
SWEEP RATIO,                    LAMBDA = .5
RATIO OF FOCAL LENGTH TO DIAMETER, F/D= 2
RATIO OF MEMBER LENGTH TO DIAMETER,L/D= .2
H/L,                                H= 1
 EPSILON=  0.050005  GAMMA=  0.025007  DELTA=  0.043309

                JOINT COORDINATES (TRIADS) AND STRUT LENGTHS
                FOR STANDARD RIB BEFORE SECOND-STAGE DEPLOYMENT

       UPPER CHORD                LOWER CHORD                CORE MEMBER

                                N=  0
                                THETA= 0.000000   0.000000      LCOR= 1.154716
            LN=  1.000000         PHI= 0.014436   0.303021
                                   RN= 20.991701 -0.989513
N=  1
THETA= 0.025003   0.500000                                      LCOR= 1.154716
   RN= 20.000000  0.000000                LN=  1.049154
 DELR=  0.000005  0.006251
                                N=  2
                                THETA= 0.049984   1.048831      LCOR= 1.154716
            LN=  0.998114         PHI= 0.014445   0.302835
                                   RN= 20.991919 -0.963514
N=  3
THETA= 0.074914   1.496835                                      LCOR= 1.154716
   RN= 19.999336  0.000000                LN=  1.045261
 DELR=  0.000809  0.056757
                                N=  4
                                THETA= 0.099782   2.091211      LCOR= 1.154716
            LN=  0.992501         PHI= 0.014472   0.302281
                                   RN= 20.992565 -0.885958
N=  5
THETA= 0.124548   2.484274                                      LCOR= 1.154716
   RN= 19.998033  0.000000                LN=  1.037571
 DELR=  0.002838  0.156873
                                N=  6
                                THETA= 0.149212   3.120880      LCOR= 1.154716
            LN=  0.983302         PHI= 0.014517   0.301374
                                   RN= 20.993611 -0.758154
N=  7
THETA= 0.173725   3.456377                                      LCOR= 1.154716
   RN= 19.996134  0.000000                LN=  1.026267
 DELR=  0.006805  0.304852
```

TABLE 2. Continued.

```
LOOP BACK ? (NO=0,YES=1)1
SWEEP RATIO,                    LAMBDA = .5
RATIO OF FOCAL LENGTH TO DIAMETER, F/D= .5
RATIO OF MEMBER LENGTH TO DIAMETER,L/D= .2
H/L,                                H= 3
 EPSILON=  0.200335  GAMMA=  0.100419  DELTA=  0.173713
```

JOINT COORDINATES (TRIADS) AND STRUT LENGTHS
FOR STANDARD RIB BEFORE SECOND-STAGE DEPLOYMENT

```
        UPPER CHORD                 LOWER CHORD                CORE MEMBER

                                N=  0
                                THETA= 0.000000   0.000000     LCOR= 3.055142
            LN=  1.000000         PHI= 0.057864   0.460732
                                   RN=  7.966797 -2.953463
N=  1
THETA= 0.100167   0.500000                                     LCOR= 3.055142
   RN=  5.000000  0.000000                LN=  1.583063
 DELR=  0.000315  0.025063
                                N=  2
                                THETA= 0.199013   1.575396     LCOR= 3.055142
            LN=  0.970715         PHI= 0.058450   0.456307
                                   RN=  7.968535 -2.797914
N=  3
THETA= 0.294712   1.450860                                     LCOR= 3.055142
   RN=  4.994963  0.000000                LN=  1.495752
 DELR=  0.013253  0.220391
                                N=  4
                                THETA= 0.386938   3.008563     LCOR= 3.055142
            LN=  0.893202         PHI= 0.060256   0.444624
                                   RN=  7.972766 -2.369930
N=  5
THETA= 0.473907   2.275927                                     LCOR= 3.055142
   RN=  4.987063  0.000000                LN=  1.349483
 DELR=  0.053258  0.562551
                                N=  6
                                THETA= 0.556327   4.212699     LCOR= 3.055142
            LN=  0.790616         PHI= 0.063436   0.429462
                                   RN=  7.977523 -1.760887
N=  7
THETA= 0.632731   2.944171                                     LCOR= 3.055142
   RN=  4.978734  0.000000                LN=  1.181443
 DELR=  0.127997  0.985072
```

TABLE 2. Continued.

```
LOOP BACK ? (NO=0,YES=1)1
SWEEP RATIO,                    LAMBDA = .5
RATIO OF FOCAL LENGTH TO DIAMETER, F/D= 1
RATIO OF MEMBER LENGTH TO DIAMETER,L/D= .2
H/L,                                H= 3
 EPSILON=  0.100042  GAMMA=  0.050052  DELTA=  0.086666

                JOINT COORDINATES (TRIADS) AND STRUT LENGTHS
                FOR STANDARD RIB BEFORE SECOND-STAGE DEPLOYMENT

       UPPER CHORD                LOWER CHORD                CORE MEMBER

                                N=  0
                                THETA= 0.000000   0.000000      LCOR= 3.055073
            LN=  1.000000         PHI= 0.028884   0.374954
                                   RN= 12.983373 -2.977957
N=  1
THETA= 0.050021   0.500000                                      LCOR= 3.055073
   RN= 10.000000  0.000000                LN=  1.296199
 DELR=  0.000040  0.012508
                                N=  2
                                THETA= 0.099875   1.294601      LCOR= 3.055073
            LN=  0.992524         PHI= 0.028956   0.374031
                                   RN= 12.983732 -2.913613
N=  3
THETA= 0.149319   1.487491                                      LCOR= 3.055073
   RN=  9.998927  0.000000                LN=  1.277213
 DELR=  0.002206  0.112336
                                N=  4
                                THETA= 0.198281   2.557795      LCOR= 3.055073
            LN=  0.970824         PHI= 0.029175   0.371352
                                   RN= 12.984753 -2.724920
N=  5
THETA= 0.246460   2.438971                                      LCOR= 3.055073
   RN=  9.996914  0.000000                LN=  1.241028
 DELR=  0.009565  0.305171
                                N=  6
                                THETA= 0.293887   3.761799      LCOR= 3.055073
            LN=  0.936908         PHI= 0.029544   0.367168
                                   RN= 12.986285 -2.424075
N=  7
THETA= 0.340226   3.335067                                      LCOR= 3.055073
   RN=  9.994192  0.000000                LN=  1.190824
 DELR=  0.026300  0.578683
```

TABLE 2. Concluded.

```
LOOP BACK ? (NO=0,YES=1)1
SWEEP RATIO,                    LAMBDA = .5
RATIO OF FOCAL LENGTH TO DIAMETER, F/D= 2
RATIO OF MEMBER LENGTH TO DIAMETER,L/D= .2
H/L,                                H= 3
 EPSILON=  0.050005  GAMMA=  0.025007  DELTA=  0.043309
```

JOINT COORDINATES (TRIADS) AND STRUT LENGTHS
FOR STANDARD RIB BEFORE SECOND-STAGE DEPLOYMENT

```
        UPPER CHORD                 LOWER CHORD                CORE MEMBER

                                N=  0
                                THETA= 0.000000   0.000000      LCOR= 3.055056
            LN=  1.000000         PHI= 0.014436   0.331891
                                   RN= 22.991677 -2.989282
N=  1
THETA= 0.025003   0.500000                                      LCOR= 3.055056
   RN= 20.000000  0.000000               LN=  1.149107
 DELR=  0.000005  0.006251
                                N=  2
                                THETA= 0.049984   1.148750      LCOR= 3.055056
            LN=  0.998124         PHI= 0.014445   0.331685
                                   RN= 22.991757 -2.960646
N=  3
THETA= 0.074914   1.496867                                      LCOR= 3.055056
   RN= 19.999760  0.000000               LN=  1.144828
 DELR=  0.000385  0.056334
                                N=  4
                                THETA= 0.099782   2.290387      LCOR= 3.055056
            LN=  0.992542         PHI= 0.014472   0.331072
                                   RN= 22.991993 -2.875233
N=  5
THETA= 0.124548   2.484430                                      LCOR= 3.055056
   RN= 19.999289  0.000000               LN=  1.136374
 DELR=  0.001582  0.155627
                                N=  6
                                THETA= 0.149212   3.418014      LCOR= 3.055056
            LN=  0.983392         PHI= 0.014517   0.330067
                                   RN= 22.992376 -2.734502
N=  7
THETA= 0.173725   3.456804                                      LCOR= 3.055056
   RN= 19.998600  0.000000               LN=  1.123951
 DELR=  0.004339  0.302424
```

TABLE 3. JOINT GEOMETRY OF QUASIPSHERICAL TETRATRUSS - ε_0 = 0.0175 rad, δ = 0.015156 rad (see Figure 10 for design values).

JOINT COORDINATES (TRIADS) AND STRUT LENGTHS
FOR STANDARD RIB BEFORE SECOND-STAGE DEPLOYMENT

UPPER CHORD		LOWER CHORD		CORE MEMBER
		N= 0		
		THETA= 0.000000	0.000000	LCOR= 1.154702
LN=	1.000000	PHI= 0.005052	0.293716	
		RN= 58.139945	-0.996346	
N= 1				
THETA= 0.008750	0.500000			LCOR= 1.154702
RN= 57.142857	0.000000	LN=	1.017397	
DELR= 0.000000	0.002188			
		N= 2		
		THETA= 0.017499	1.017359	LCOR= 1.154702
LN=	0.999770	PHI= 0.005052	0.293694	
		RN= 58.139971	-0.987470	
N= 3				
THETA= 0.026246	1.499615			LCOR= 1.154702
RN= 57.142779	0.000000	LN=	1.016931	
DELR= 0.000085	0.019759			
		N= 4		
		THETA= 0.034991	2.033942	LCOR= 1.154702
LN=	0.999080	PHI= 0.005053	0.293627	
		RN= 58.140048	-0.960861	
N= 5				
THETA= 0.043730	2.498078			LCOR= 1.154702
RN= 57.142623	0.000000	LN=	1.016000	
DELR= 0.000273	0.054864			
		N= 6		
		THETA= 0.052466	3.048976	LCOR= 1.154702
LN=	0.997932	PHI= 0.005055	0.293515	
		RN= 58.140178	-0.916577	
N= 7				
THETA= 0.061195	3.494624			LCOR= 1.154702
RN= 57.142389	0.000000	LN=	1.014607	
DELR= 0.000600	0.107428			
		N= 8		
		THETA= 0.069917	4.061696	LCOR= 1.154702
LN=	0.996329	PHI= 0.005058	0.293360	
		RN= 58.140357	-0.854709	
N= 9				
THETA= 0.078631	4.488498			LCOR= 1.154702
RN= 57.142079	0.000000	LN=	1.012757	
DELR= 0.001115	0.177336			
		N= 10		
		THETA= 0.087336	5.071342	LCOR= 1.154702
LN=	0.994278	PHI= 0.005062	0.293161	
		RN= 58.140587	-0.775390	
N= 11				
THETA= 0.096031	5.478953			LCOR= 1.154702
RN= 57.141694	0.000000	LN=	1.010454	
DELR= 0.001884	0.264440			
		N= 12		
		THETA= 0.104716	6.077167	LCOR= 1.154702
LN=	0.991783	PHI= 0.005066	0.292918	
		RN= 58.140865	-0.678786	
N= 13				
THETA= 0.113388	6.465256			LCOR= 1.154702
RN= 57.141236	0.000000	LN=	1.007706	
DELR= 0.002982	0.368555			
		N= 14		
		THETA= 0.122048	7.078440	LCOR= 1.154702
LN=	0.988853	PHI= 0.005071	0.292634	
		RN= 58.141190	-0.565098	

TABLE 3. Continued.

```
ETA= 0.122048   7.078440      LCOR= 1.154702
             LN=  0.988853     PHI= 0.005071   0.292634
                                RN= 58.141190 -0.565098
N= 15
THETA= 0.130694   7.446689                                  LCOR= 1.154702
   RN= 57.140707  0.000000              LN=  1.004521
 DELR=  0.004499  0.489462
                                N= 16
                                THETA= 0.139326   8.074444   LCOR= 1.154702
             LN=  0.985495       PHI= 0.005077   0.292308
                                 RN= 58.141561 -0.434561
N= 17
THETA= 0.147941   8.422552                                  LCOR= 1.154702
   RN= 57.140108  0.000000              LN=  1.000909
 DELR=  0.006535  0.626907
                                N= 18
                                THETA= 0.156541   9.064482   LCOR= 1.154702
             LN=  0.981721       PHI= 0.005083   0.291942
                                 RN= 58.141976 -0.287442
N= 19
THETA= 0.165122   9.392166                                  LCOR= 1.154702
   RN= 57.139443  0.000000              LN=  0.996879
 DELR=  0.009200  0.780608
                                N= 20
                                THETA= 0.173687  10.047877   LCOR= 1.154702
             LN=  0.977540       PHI= 0.005091   0.291536
                                 RN= 58.142432 -0.124040
N= 21
THETA= 0.182230  10.354874                                  LCOR= 1.154702
   RN= 57.138714  0.000000              LN=  0.992444
 DELR=  0.012610  0.950249
                                N= 22
                                THETA= 0.190756  11.023979   LCOR= 1.154702
             LN=  0.972965       PHI= 0.005099   0.291092
                                 RN= 58.142927  0.055318
N= 23
THETA= 0.199259  11.310043                                  LCOR= 1.154702
   RN= 57.137923  0.000000              LN=  0.987615
 DELR=  0.016889  1.135490
                                N= 24
                                THETA= 0.207742  11.992160   LCOR= 1.154702
             LN=  0.968009       PHI= 0.005108   0.290611
                                 RN= 58.143460  0.250278
N= 25
THETA= 0.216201  12.257066                                  LCOR= 1.154702
   RN= 57.137075  0.000000              LN=  0.982407
 DELR=  0.022167  1.335961
                                N= 26
                                THETA= 0.224639  12.951819   LCOR= 1.154702
             LN=  0.962686       PHI= 0.005118   0.290094
                                 RN= 58.144027  0.460461
```

TABLE 3. Concluded.

```
N= 27
THETA= 0.233050  13.195365                                  LCOR= 1.154702
   RN= 57.136171  0.000000                LN=  0.976833
 DELR=  0.028574  1.551271
                                  N= 28
                                  THETA= 0.241439  13.902385      LCOR= 1.154702
            LN=  0.957009           PHI= 0.005128   0.289543
                                     RN= 58.144626  0.685463
N= 29
THETA= 0.249800  14.124391                                  LCOR= 1.154702
   RN= 57.135216  0.000000                LN=  0.970909
 DELR=  0.036244  1.781007
                                  N= 30
                                  THETA= 0.258137  14.843317      LCOR= 1.154702
            LN=  0.950995           PHI= 0.005140   0.288960
                                     RN= 58.145254  0.924861
N= 31
THETA= 0.266445  15.043624                                  LCOR= 1.154702
   RN= 57.134213  0.000000                LN=  0.964650
 DELR=  0.045312  2.024733
```

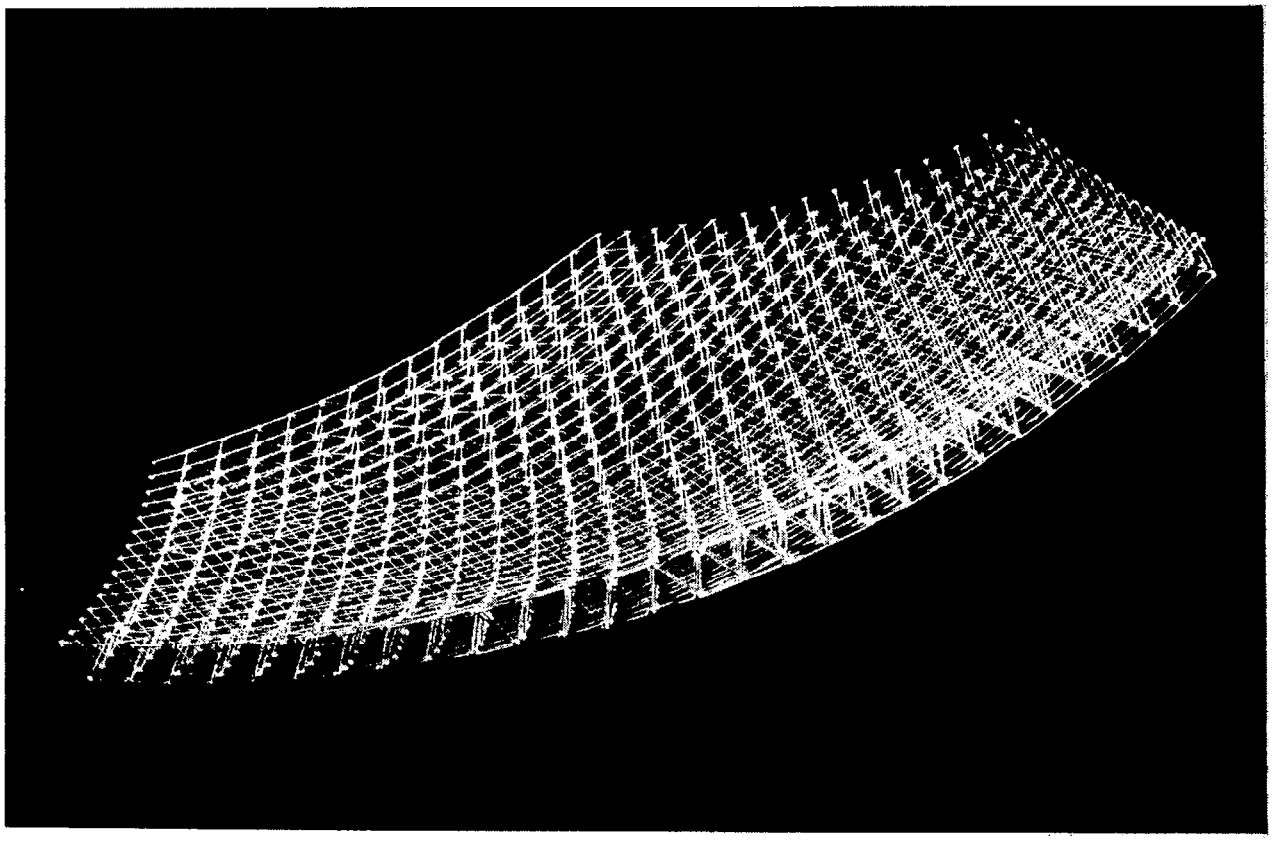

Figure 1. Tetrahedral truss reflector structure. *P001*

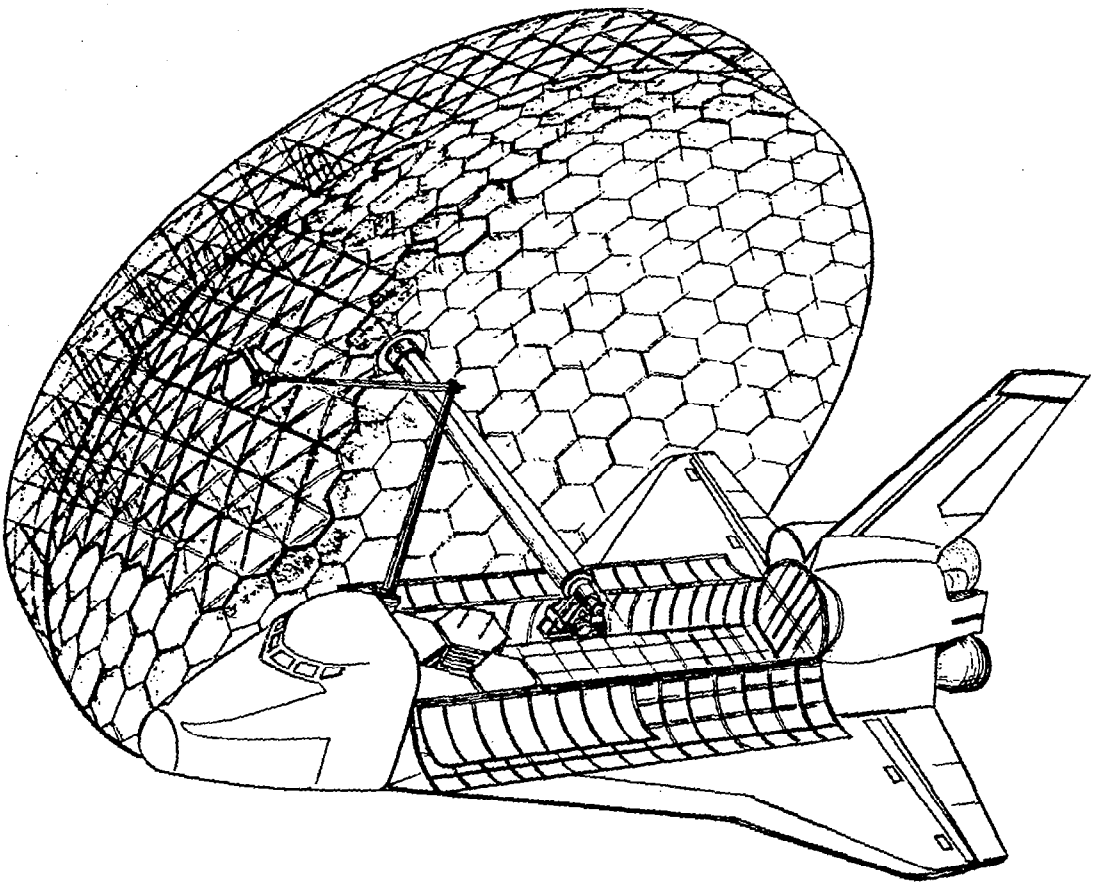

Figure 2. Assembly of surface panels to erected truss.

008A

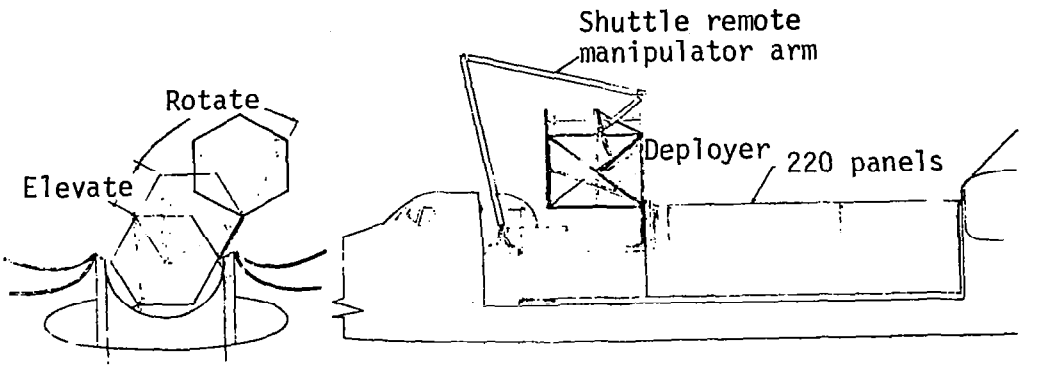

a. Module deployment

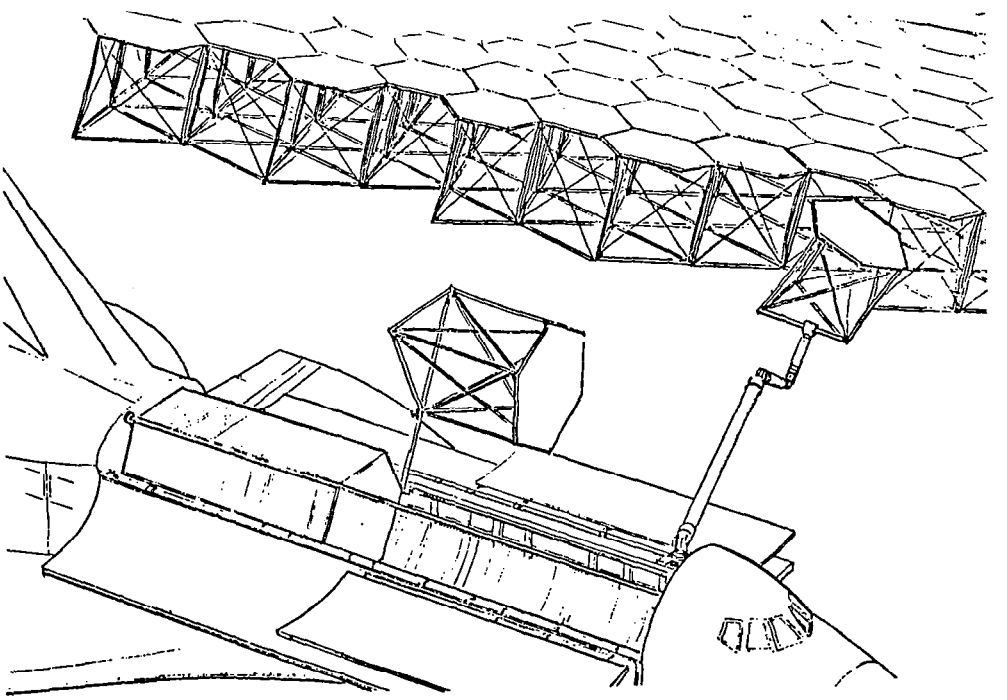

b. Reflector assembly

Figure 3. Assembly from deployable modules.

030A

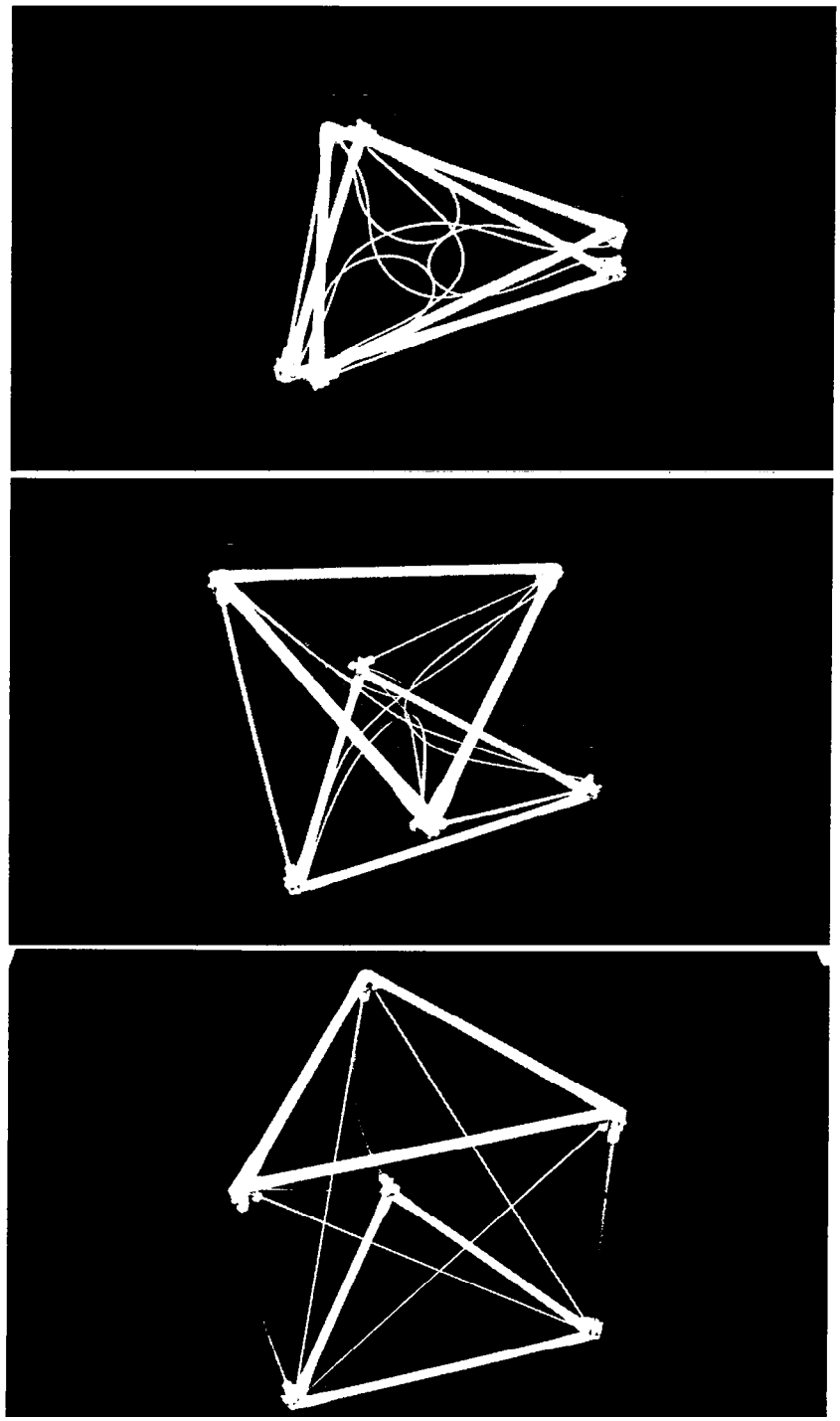

Figure 4. Astrocell module.

P002

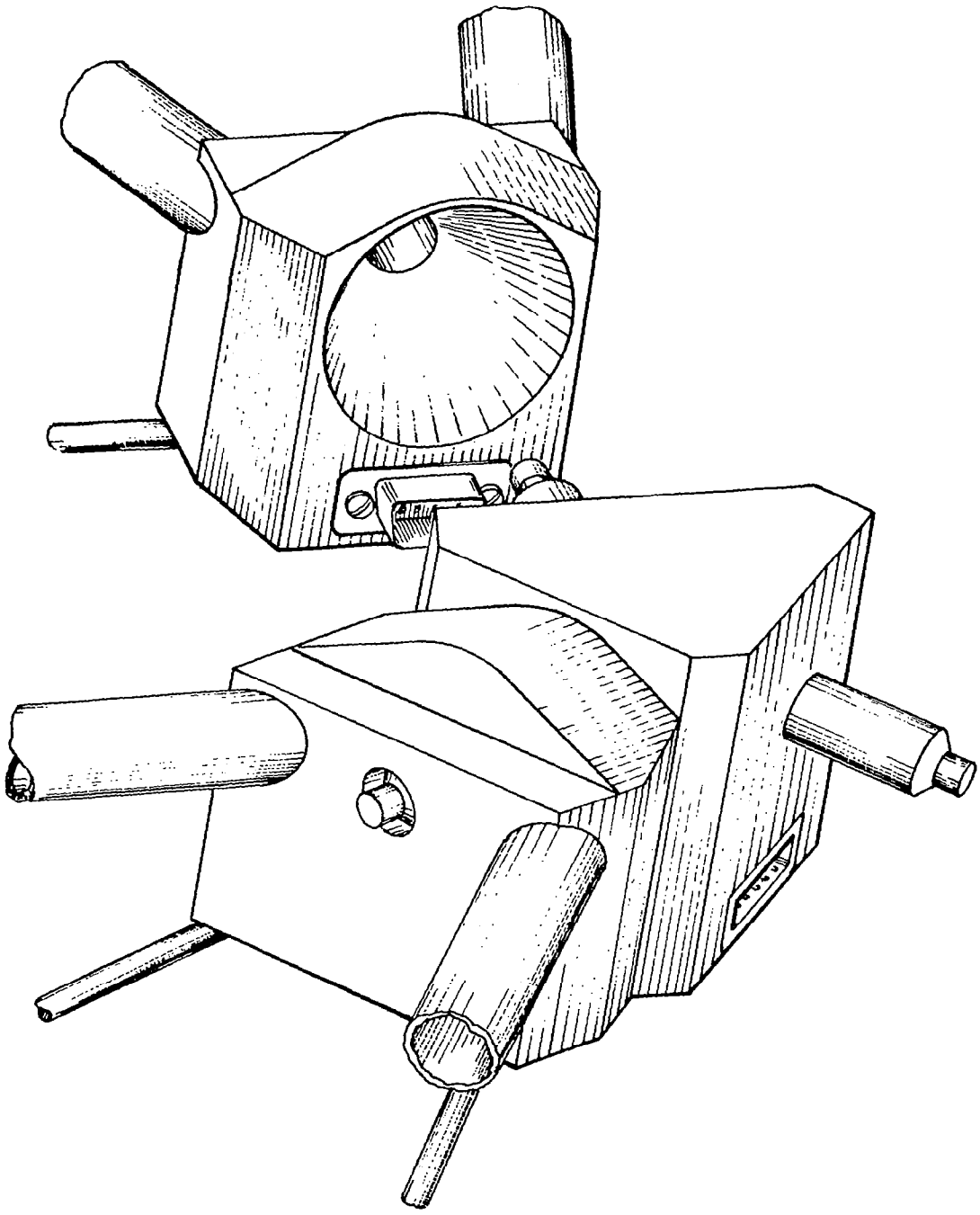

Figure 5. Intermodule connections.

011A

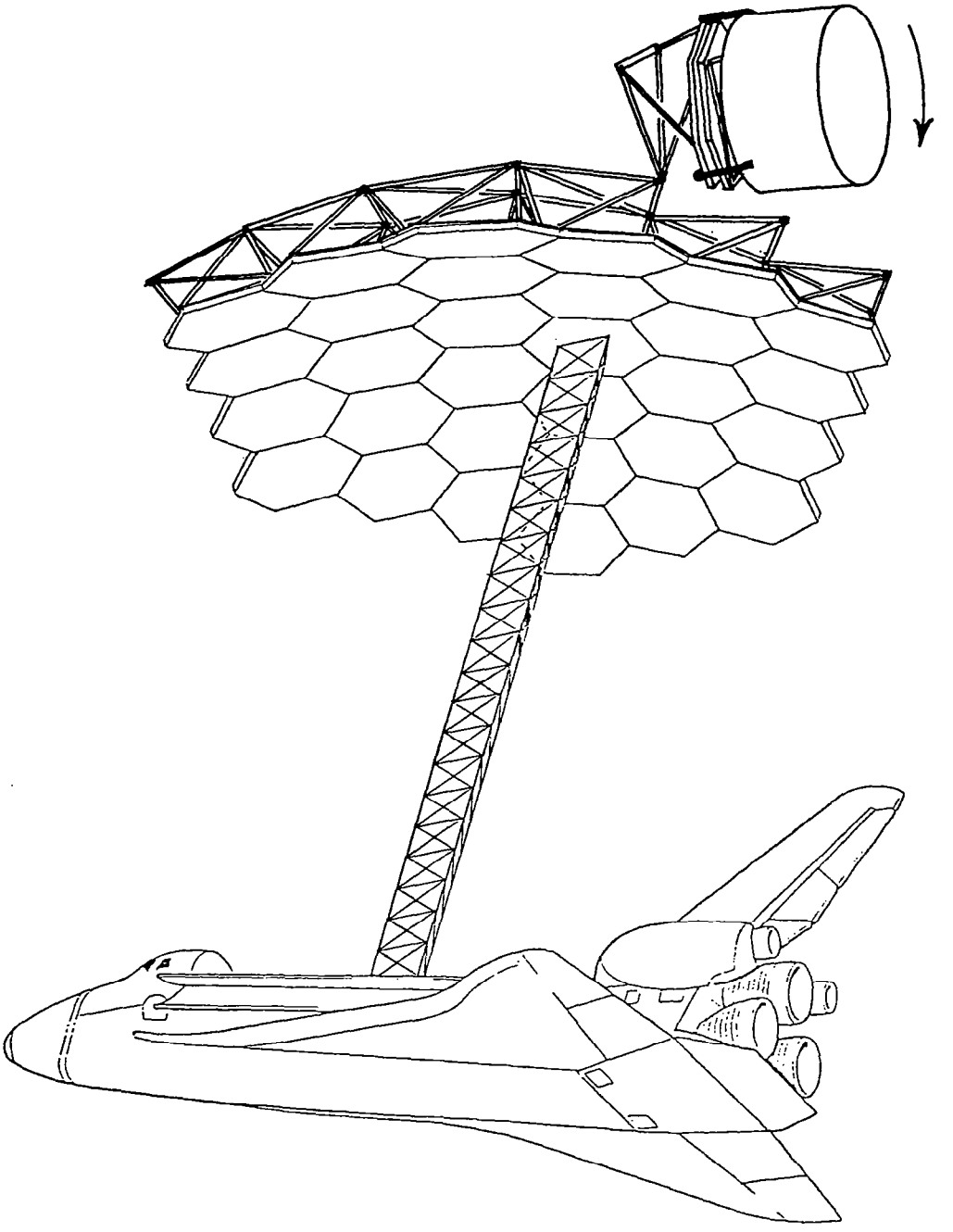

Figure 6. Deployable solid panel integrated truss. *001A*

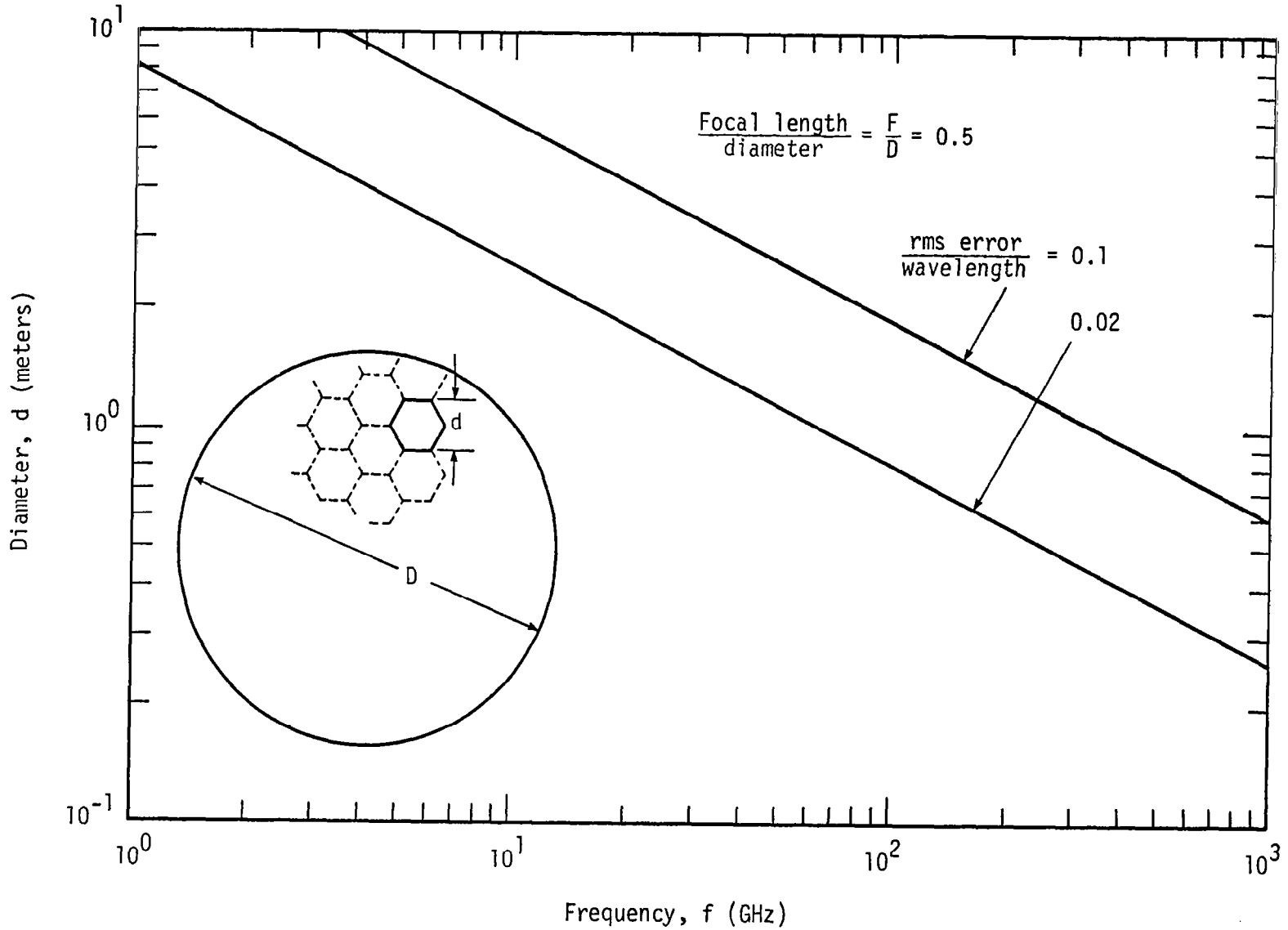

Figure 7. Diameter of constant-curvature spherical segments required for a 30-m-diameter paraboloidal reflector to operate at various frequencies.

002A

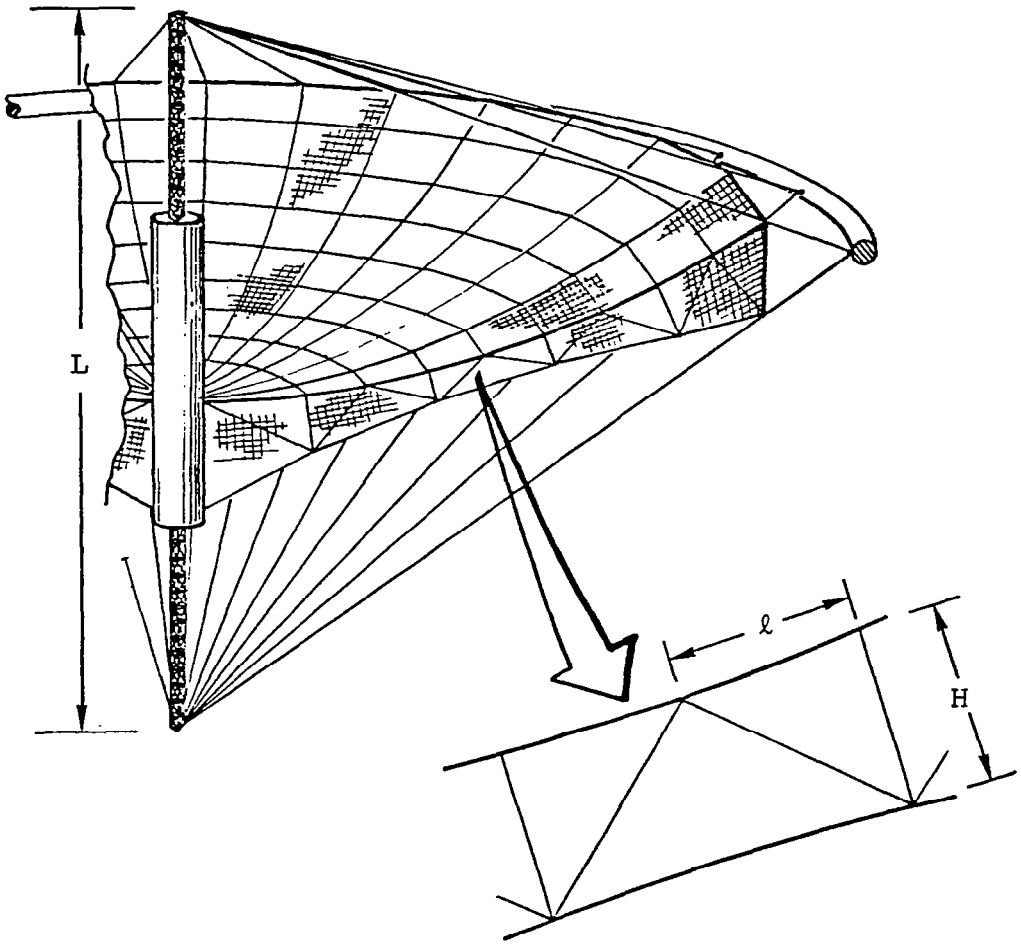

Figure 8. Pretensioned truss configuration.

028A

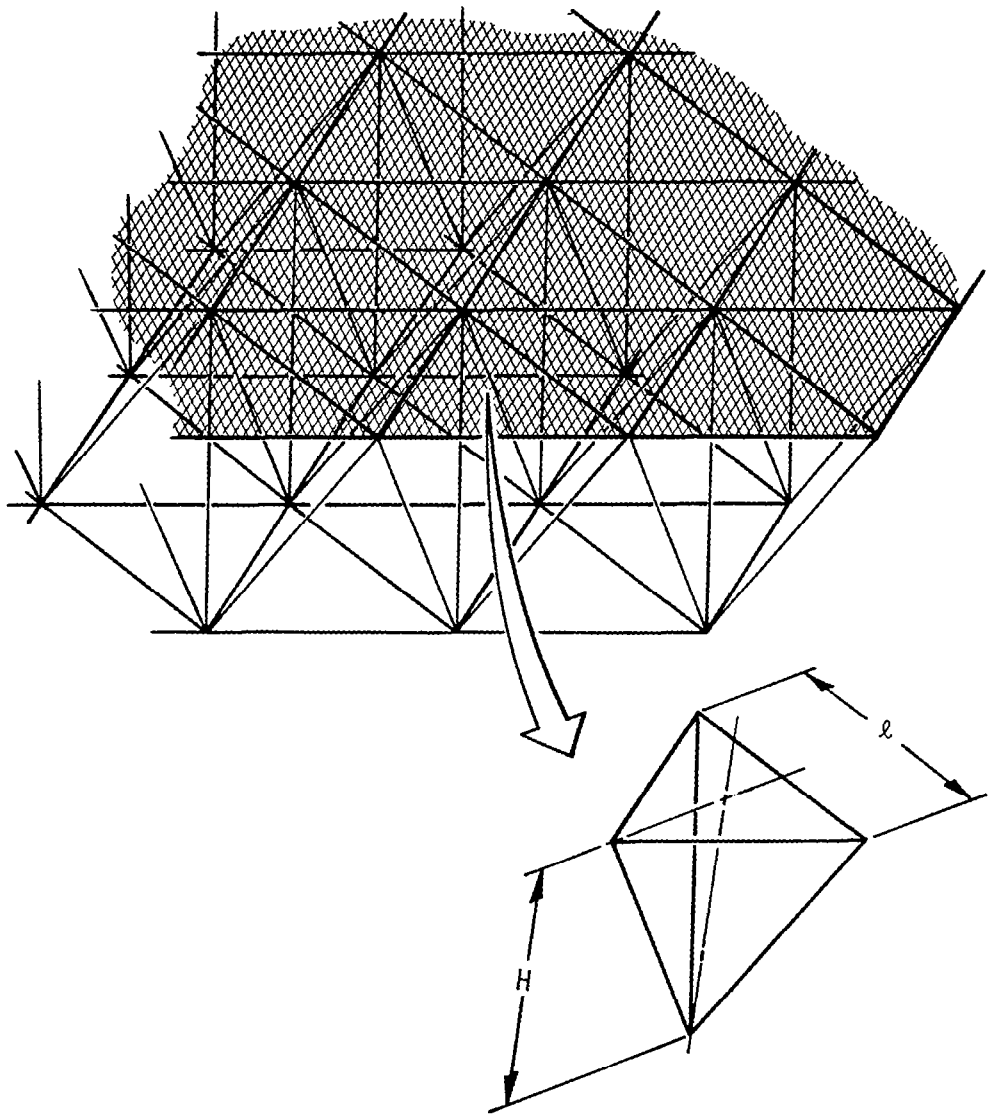

Figure 9. Tetrahedral truss configuration.

016A

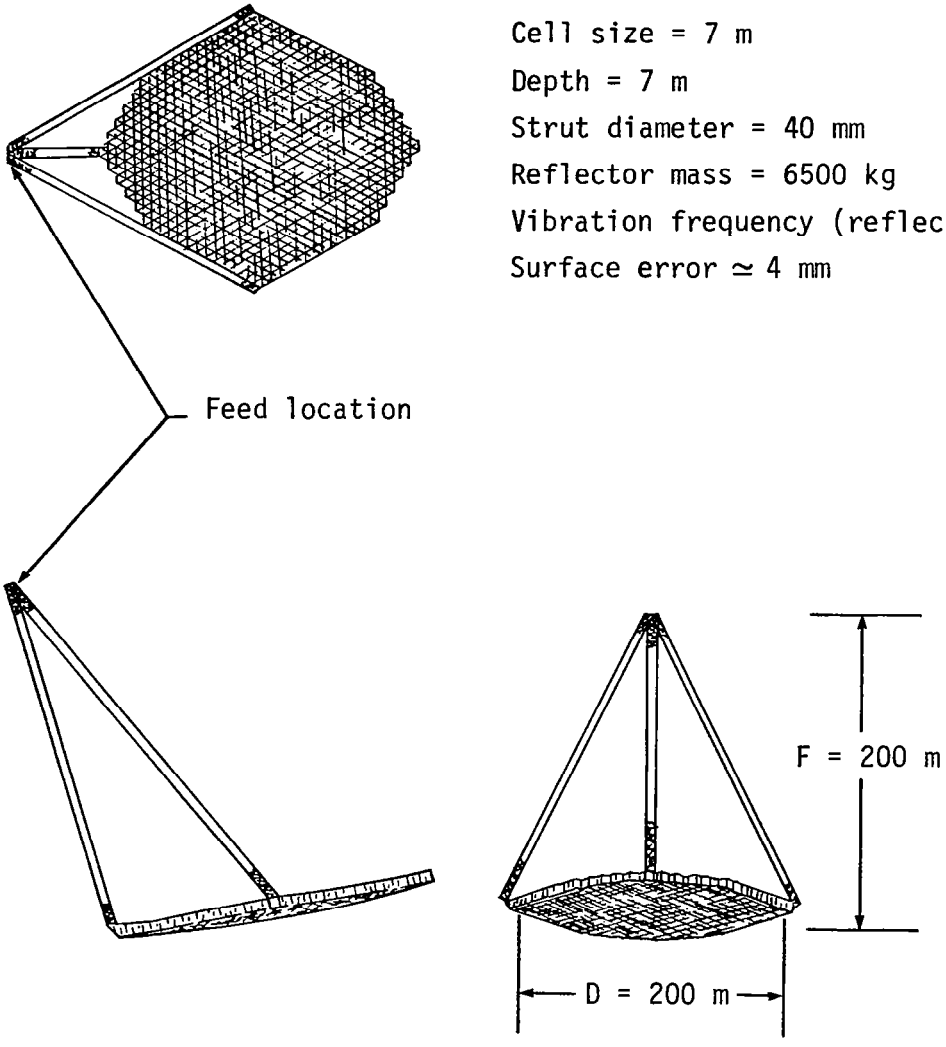

Figure 10. 200-meter-diameter deployable antenna. *003A*

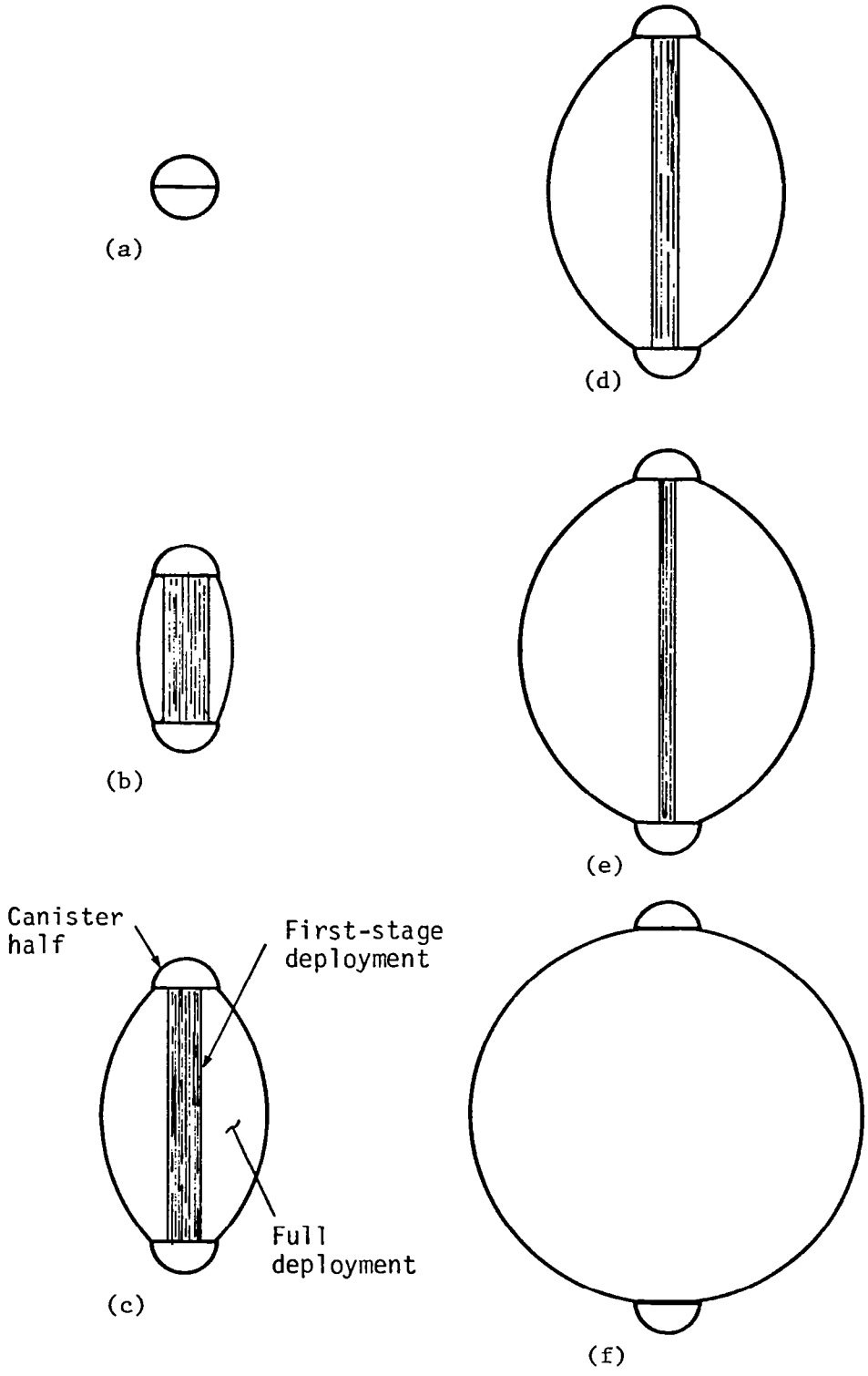

Figure 11. Schematic diagram of sequential deployment. *004A*

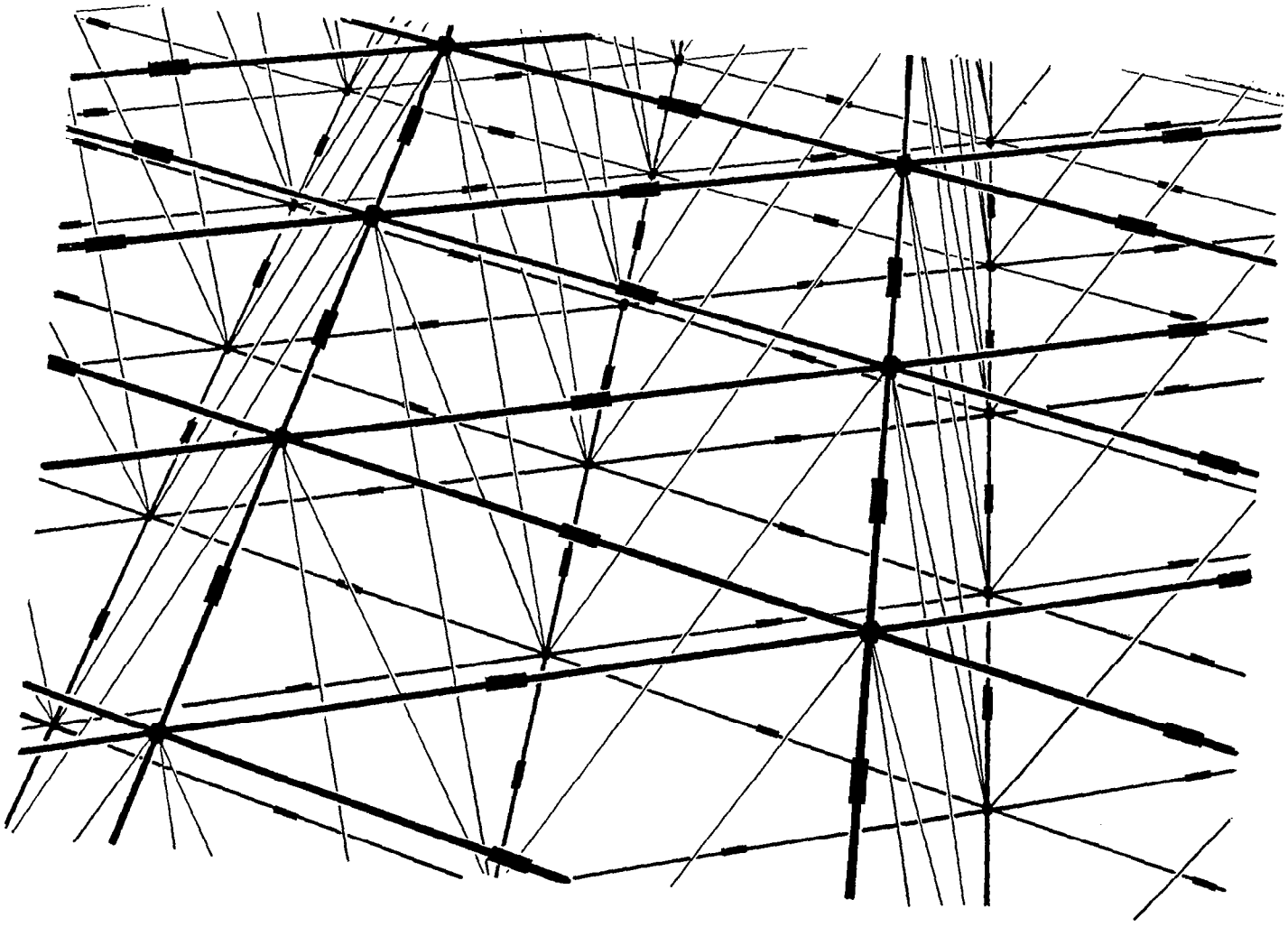

Figure 12. Tetrahedral truss structure showing joint locations. *012A*

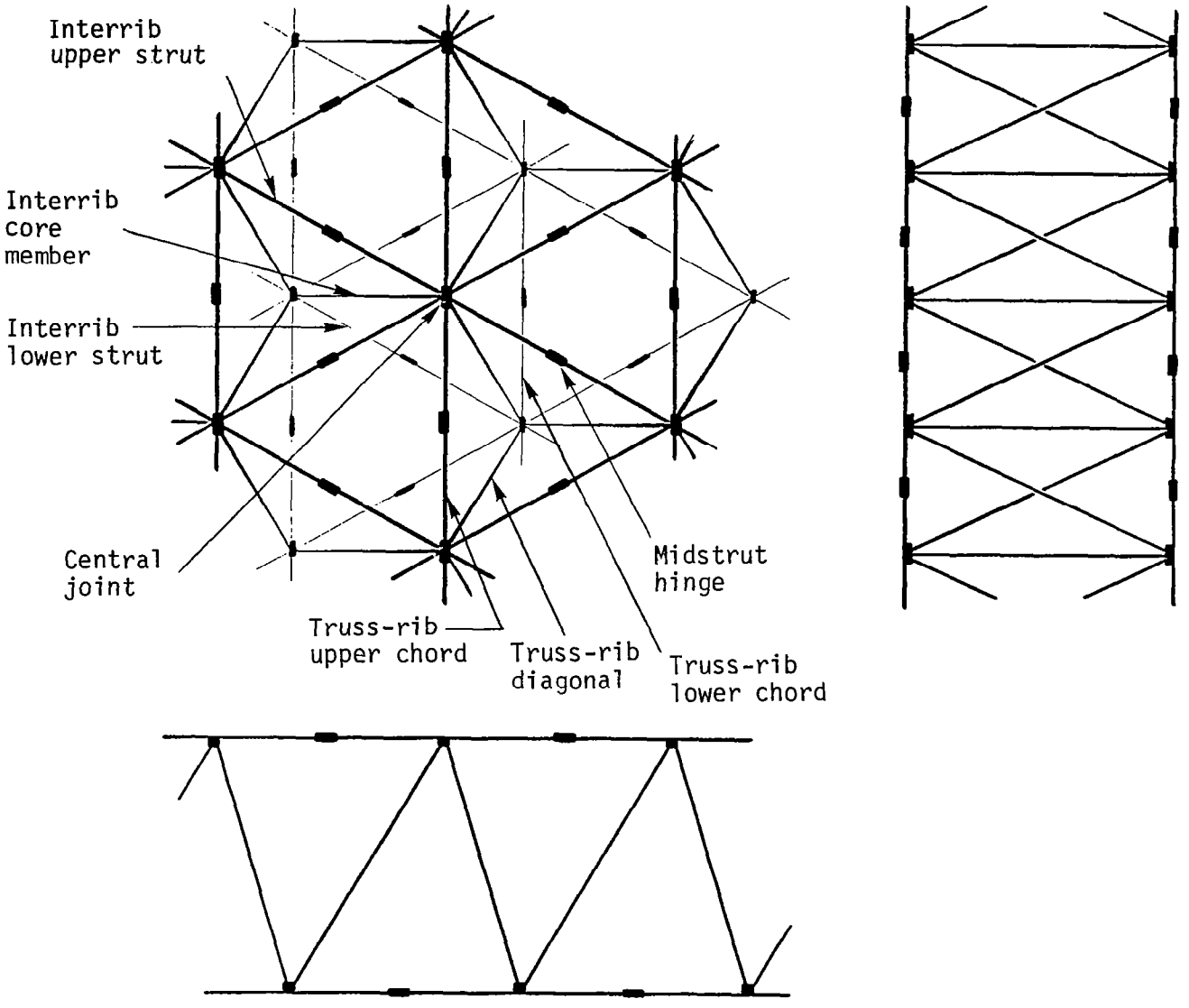

Figure 13. Tetrahedral truss nomenclature.

013A

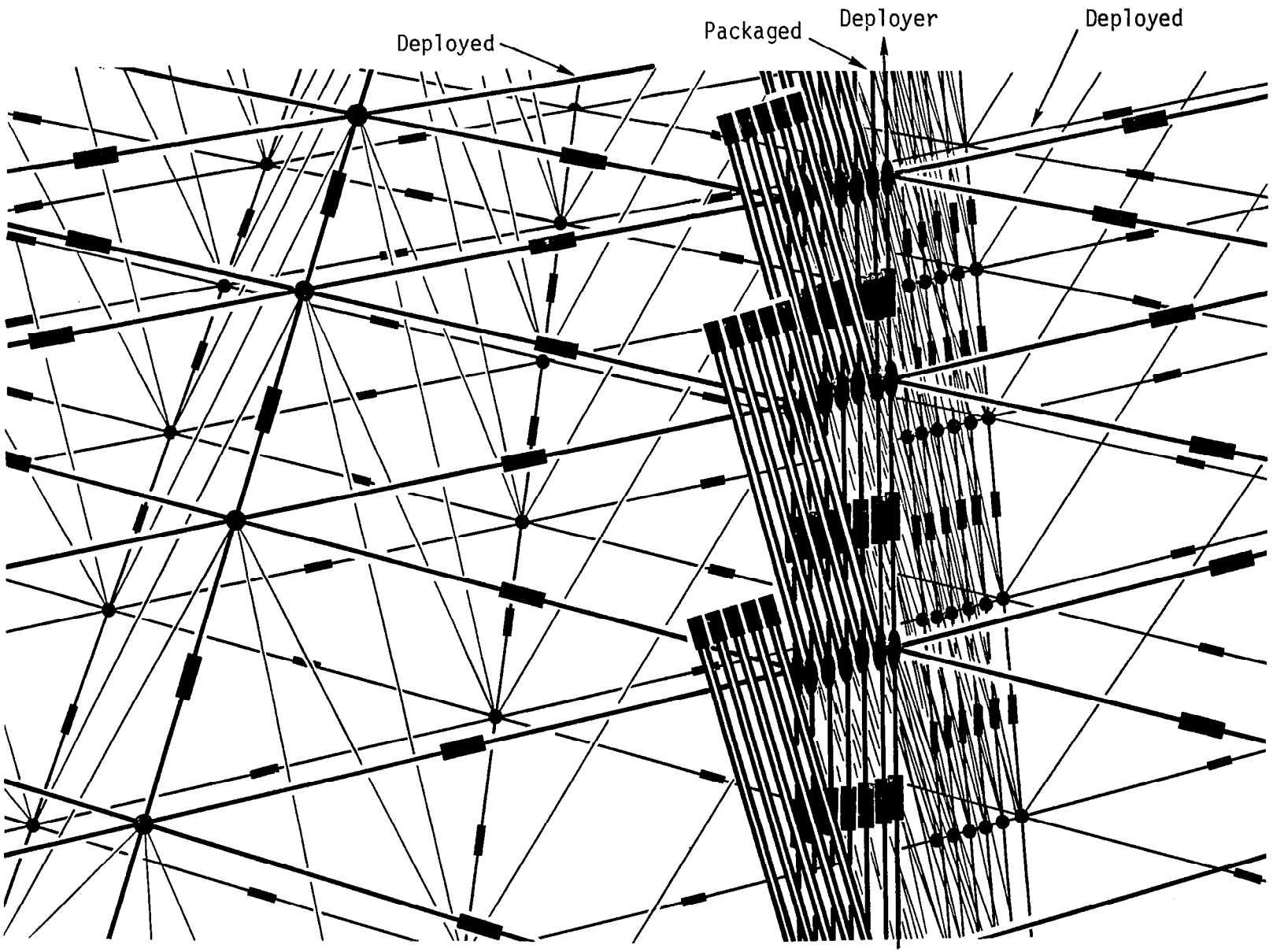

Figure 14. Partially deployed structure.

015A

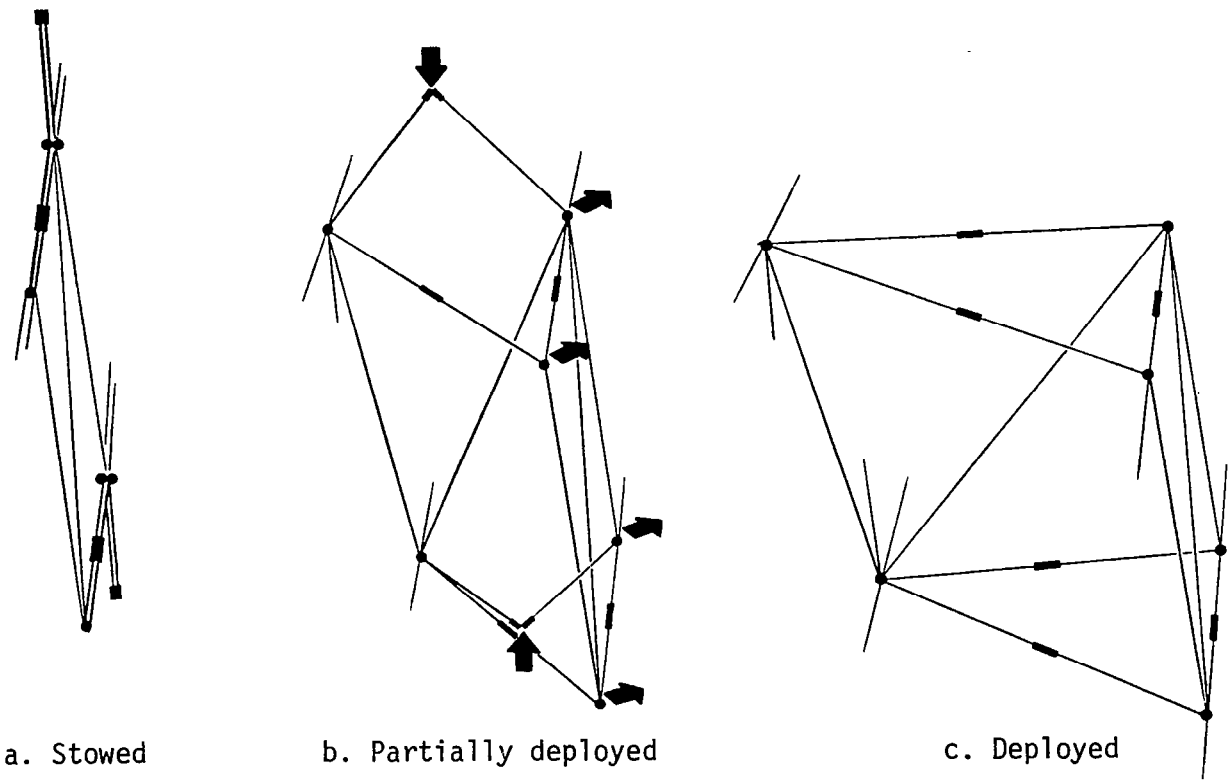

Figure 15. Second-stage deployment. *014A*

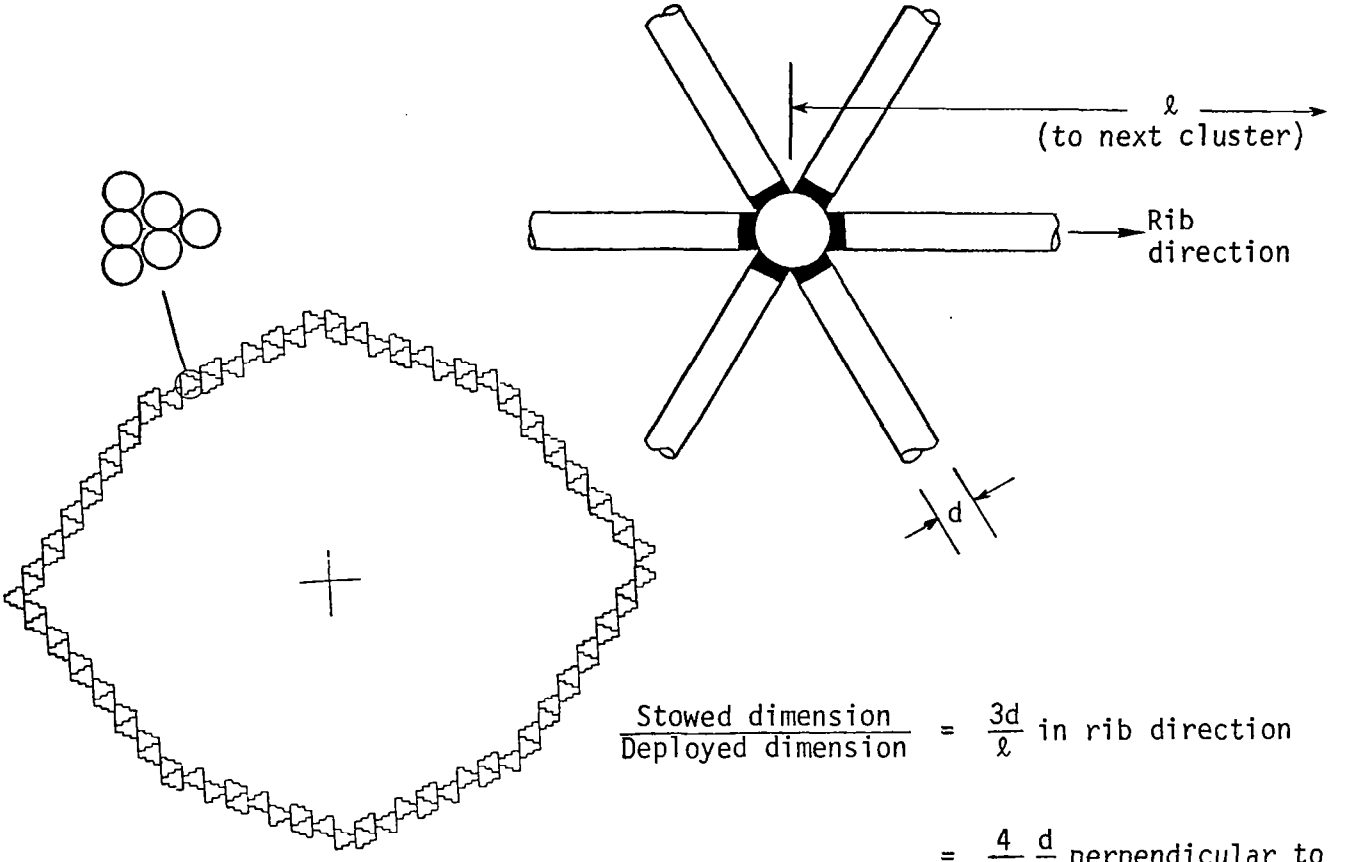

$$\frac{\text{Stowed dimension}}{\text{Deployed dimension}} = \frac{3d}{\ell} \text{ in rib direction}$$

$$= \frac{4}{\sqrt{3}}\frac{d}{\ell} \text{ perpendicular to rib direction}$$

Figure 16. Surface-member packaging. *027A*

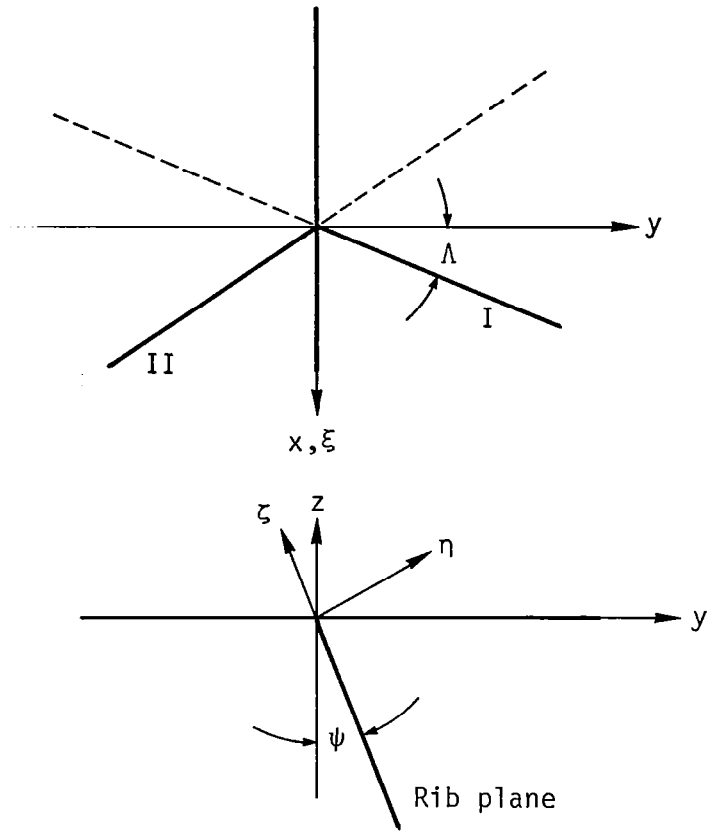

(a) Truss members

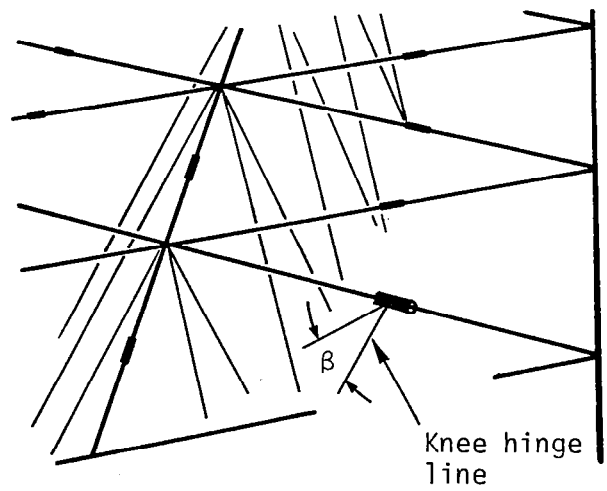

(b) Knee-hinge orientation

Figure 17. Coordinates and angles. 005A

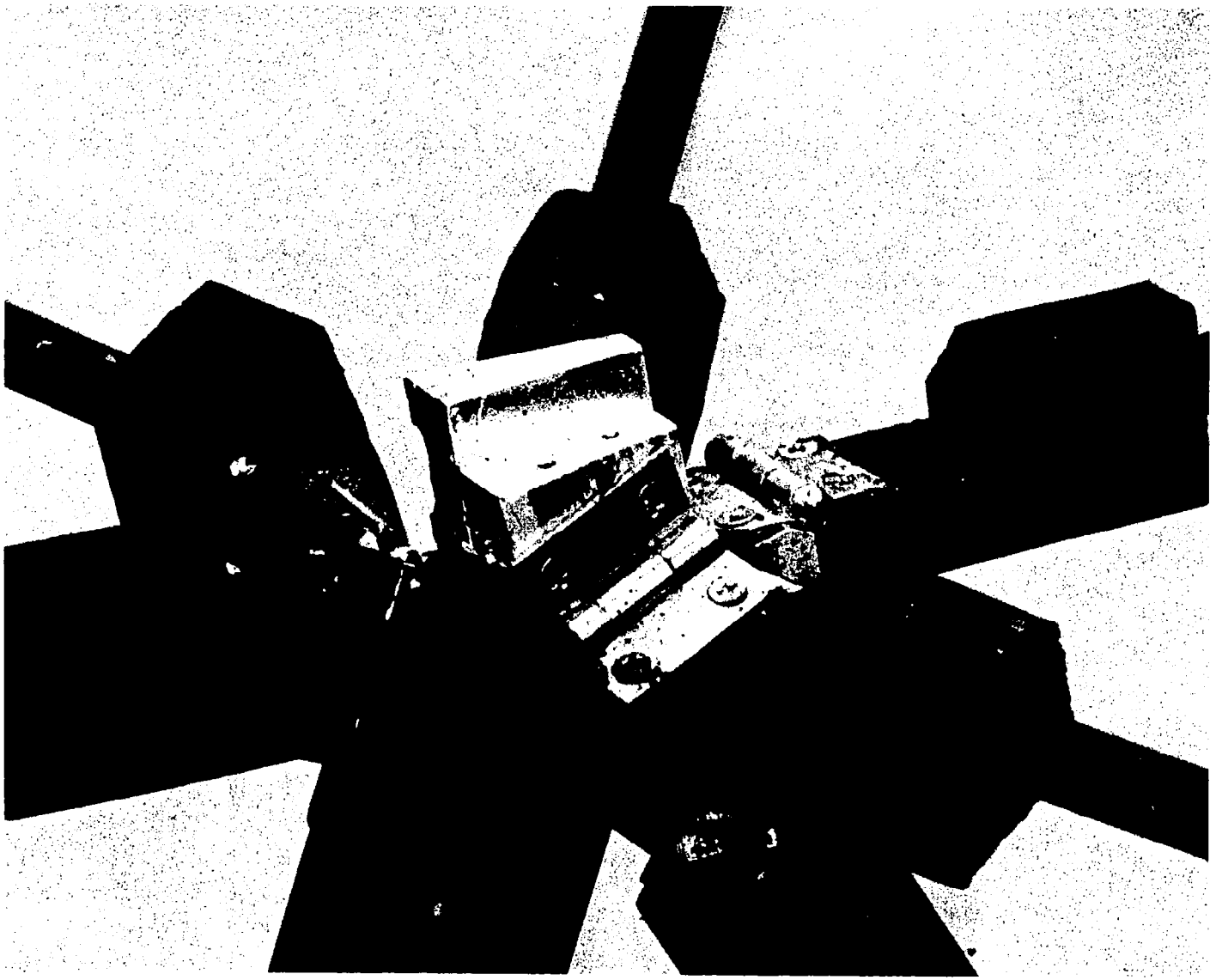

Figure 18. Detail of concept visualization model.

P003

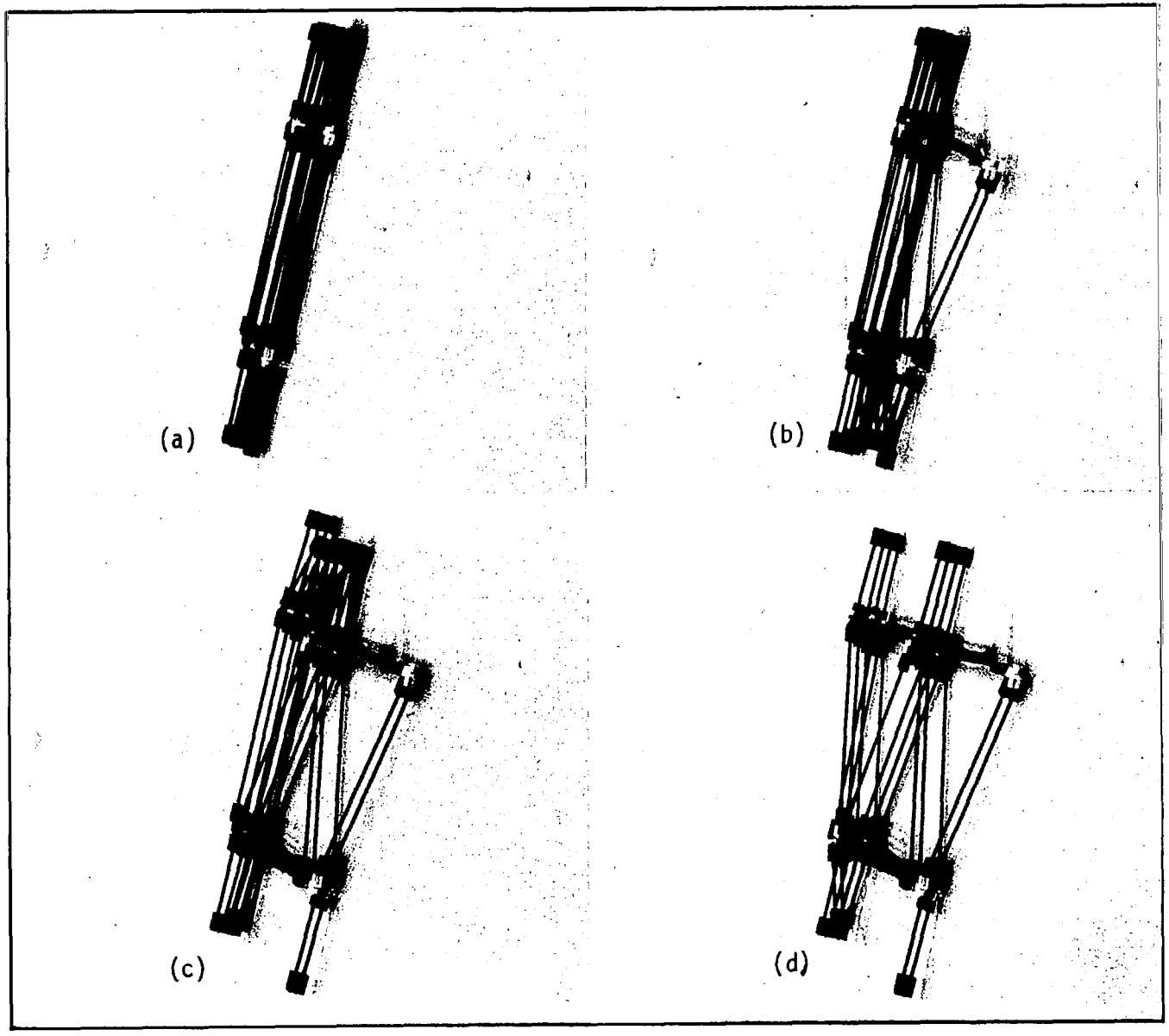

Figure 19. Deployment sequence of a sequentially deployable tetrahedral truss structure.

P004

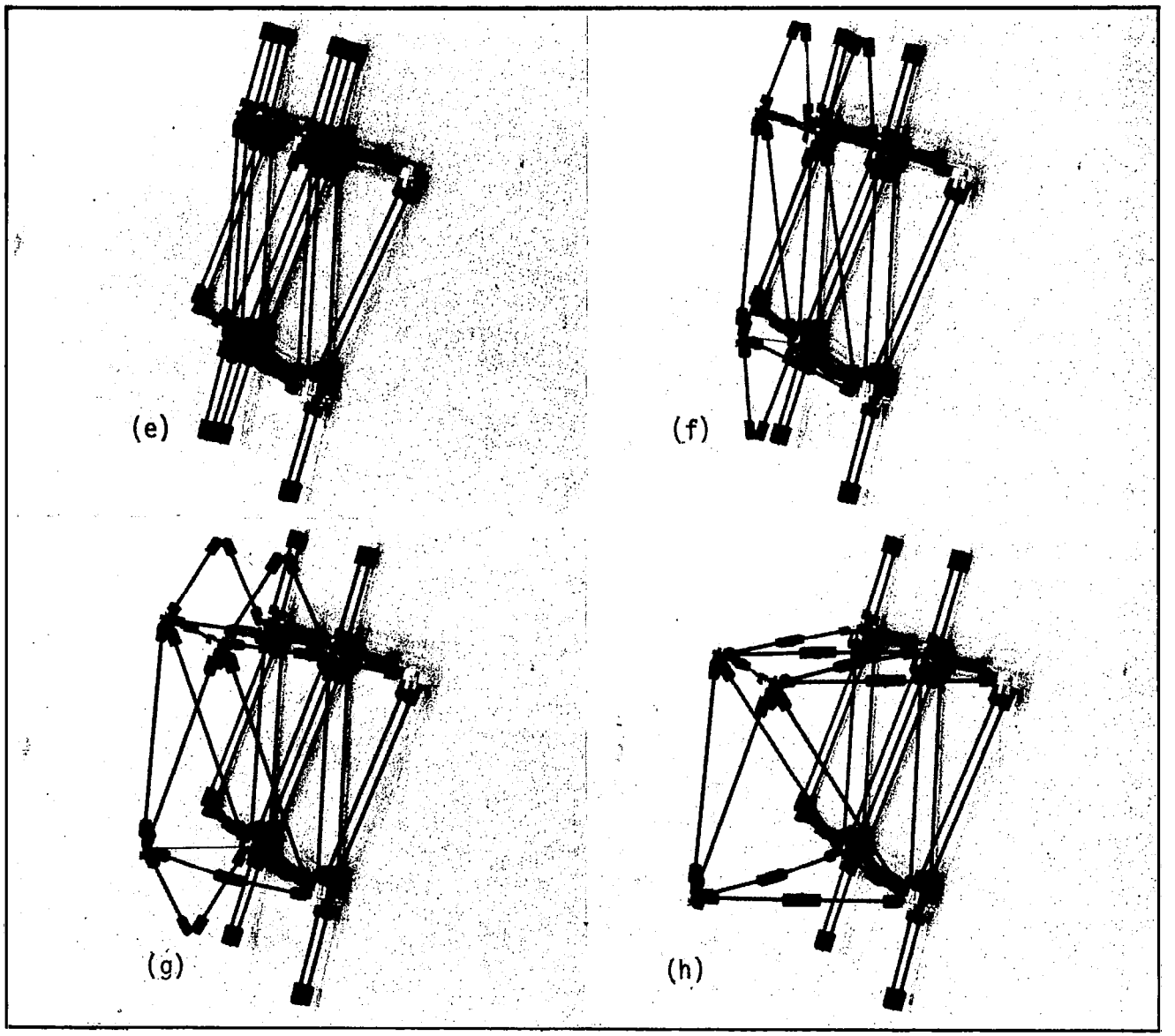

Figure 19. Continued.

P005

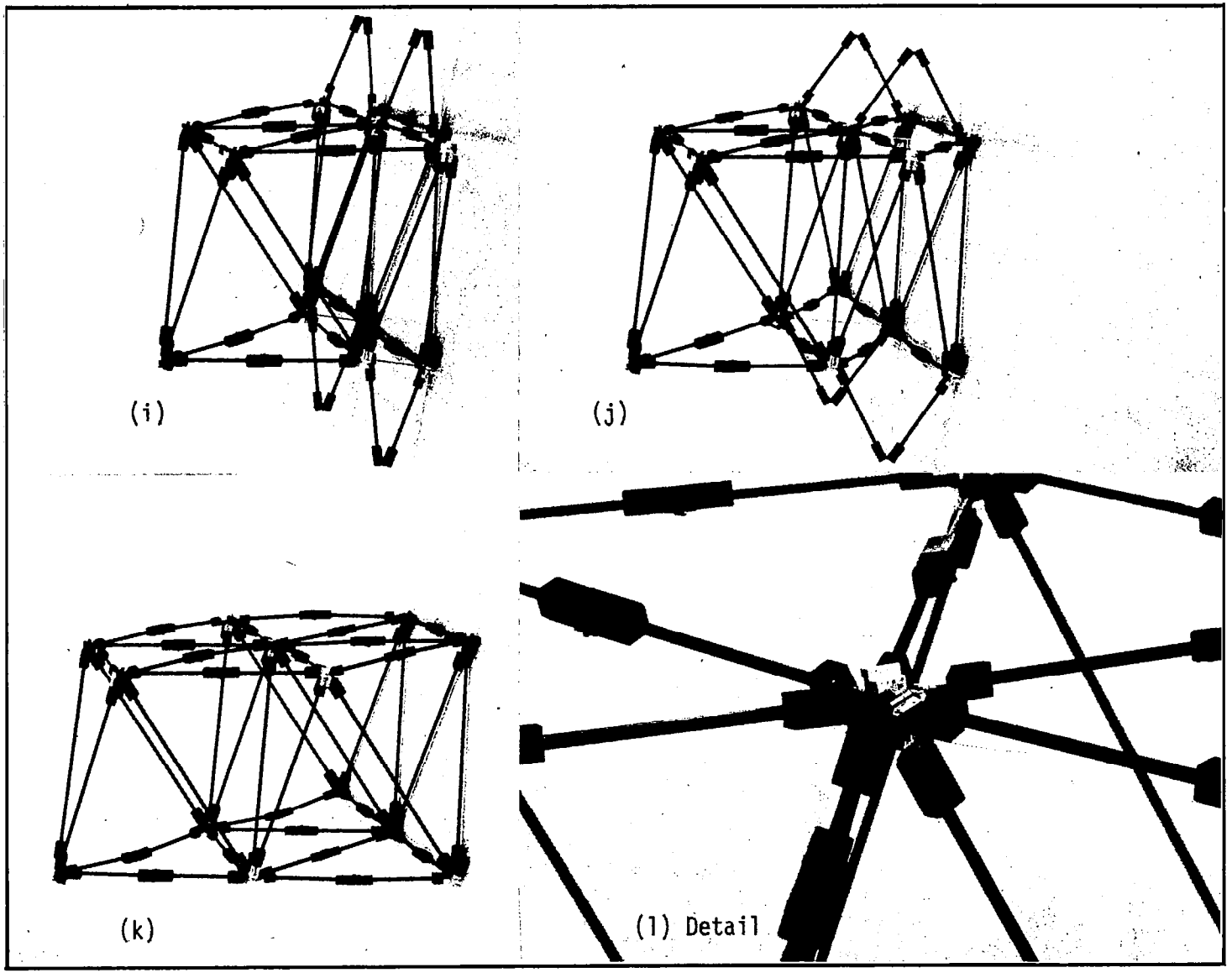

Figure 19. Concluded.

P006

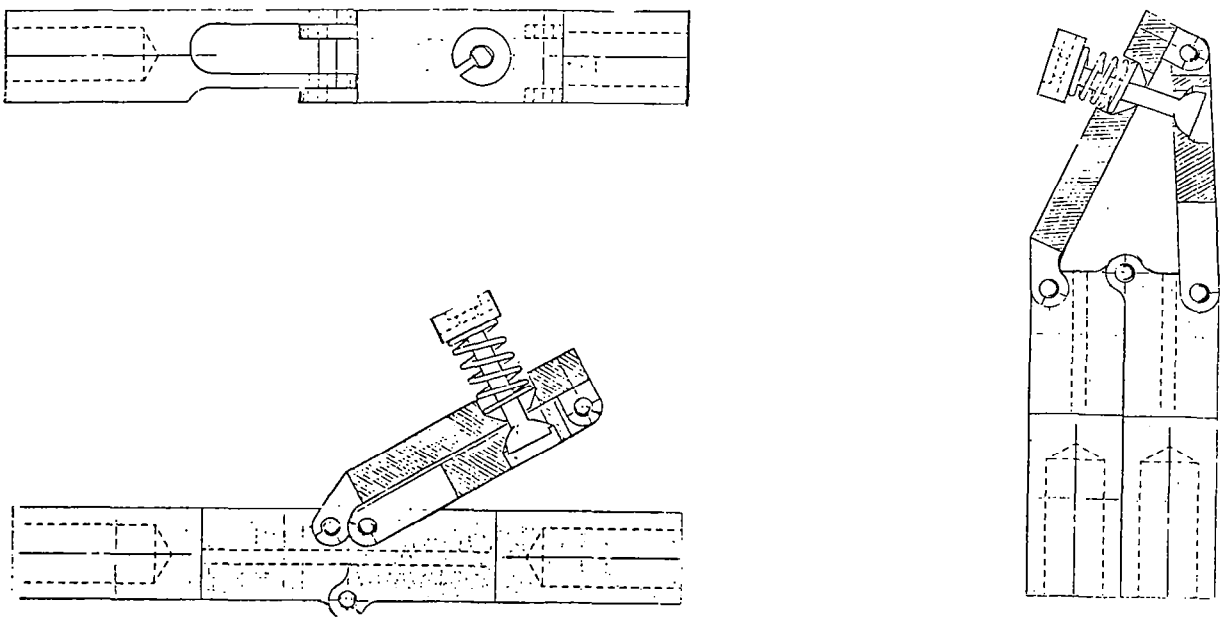

Figure 20. Almost-over-center hinge. *026A*

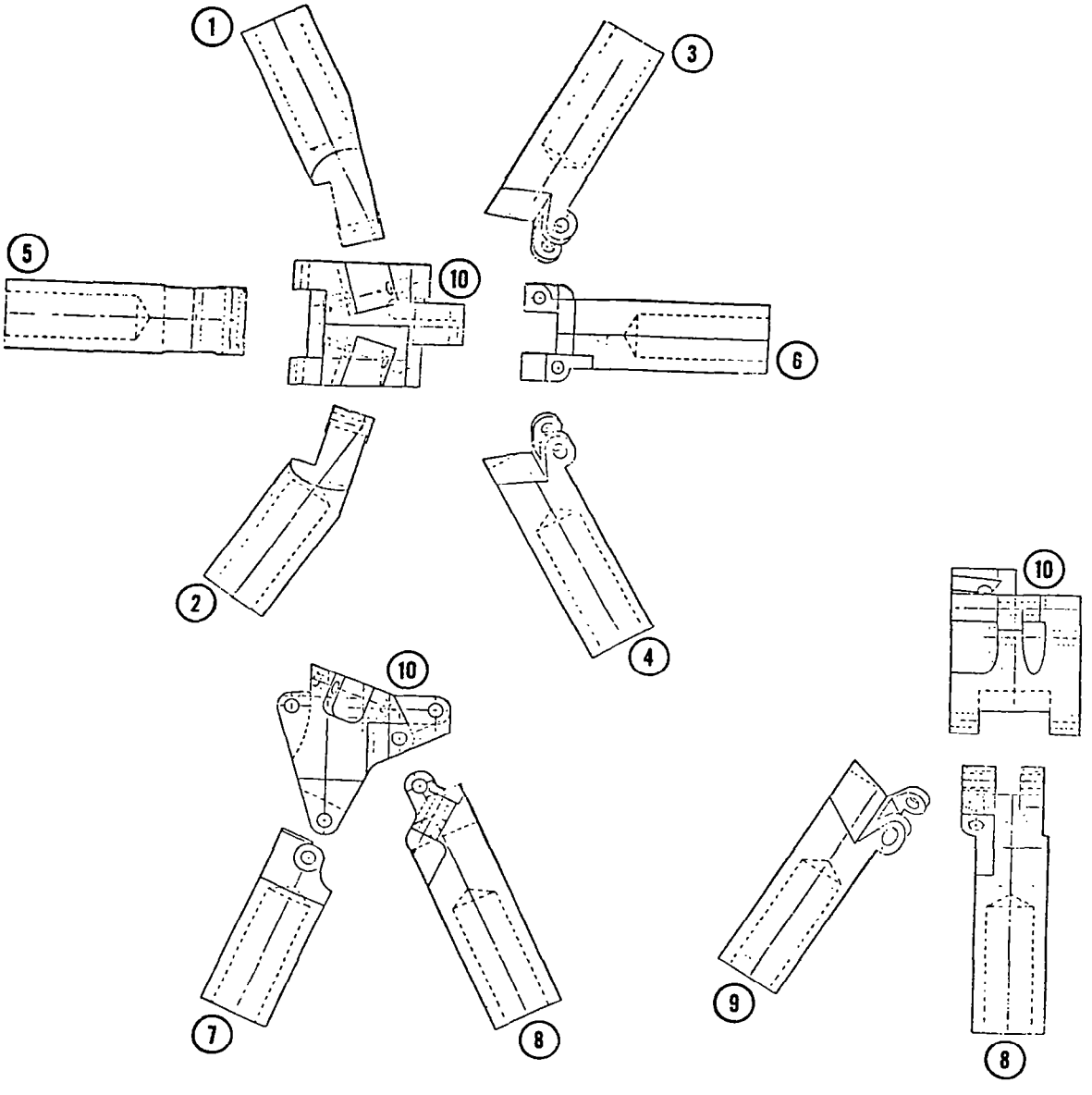

Figure 21. Nine-member joint. *025A*

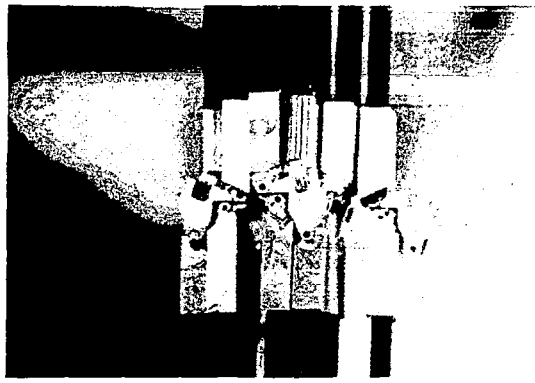

a. Fully packaged

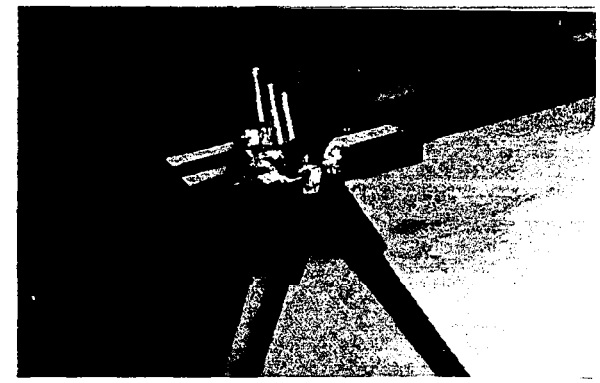

b. Partial deployment

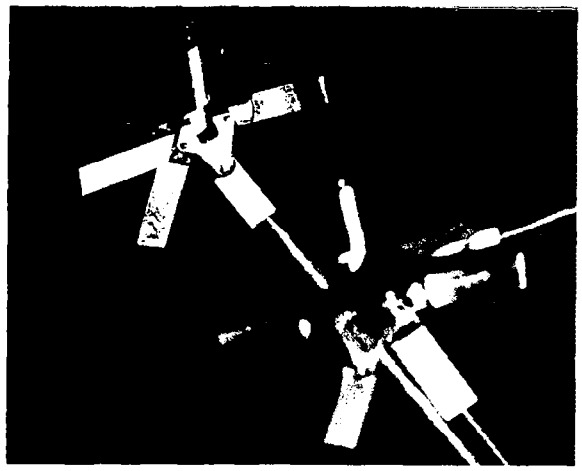

c. Transition

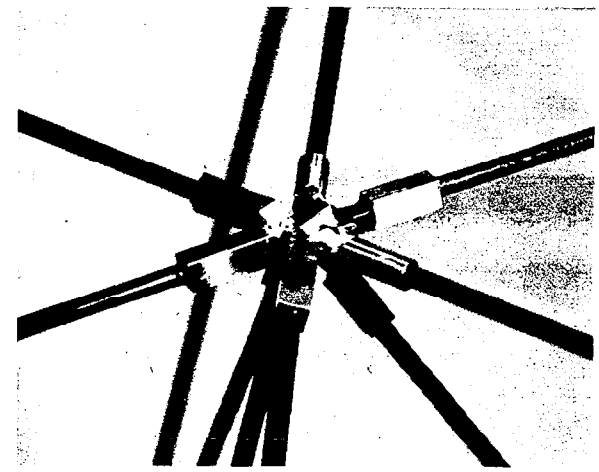

d. Fully deployed

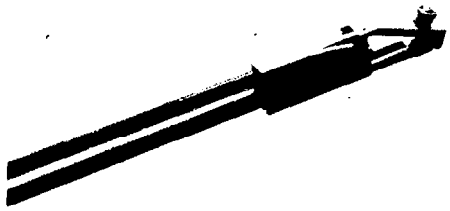

e. Folded knee hinge

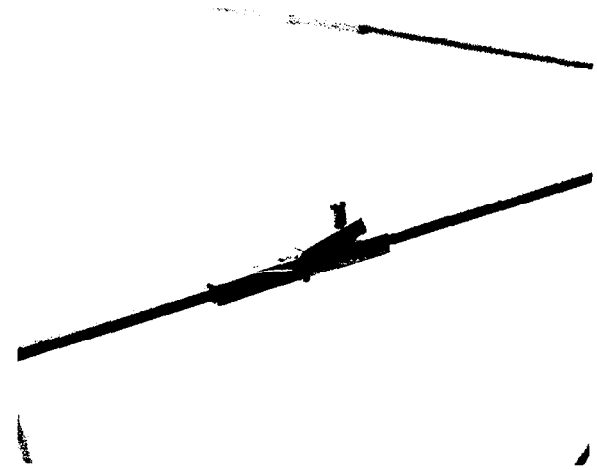

f. Deployed knee hinge

Figure 22. Hinge details. *P007*

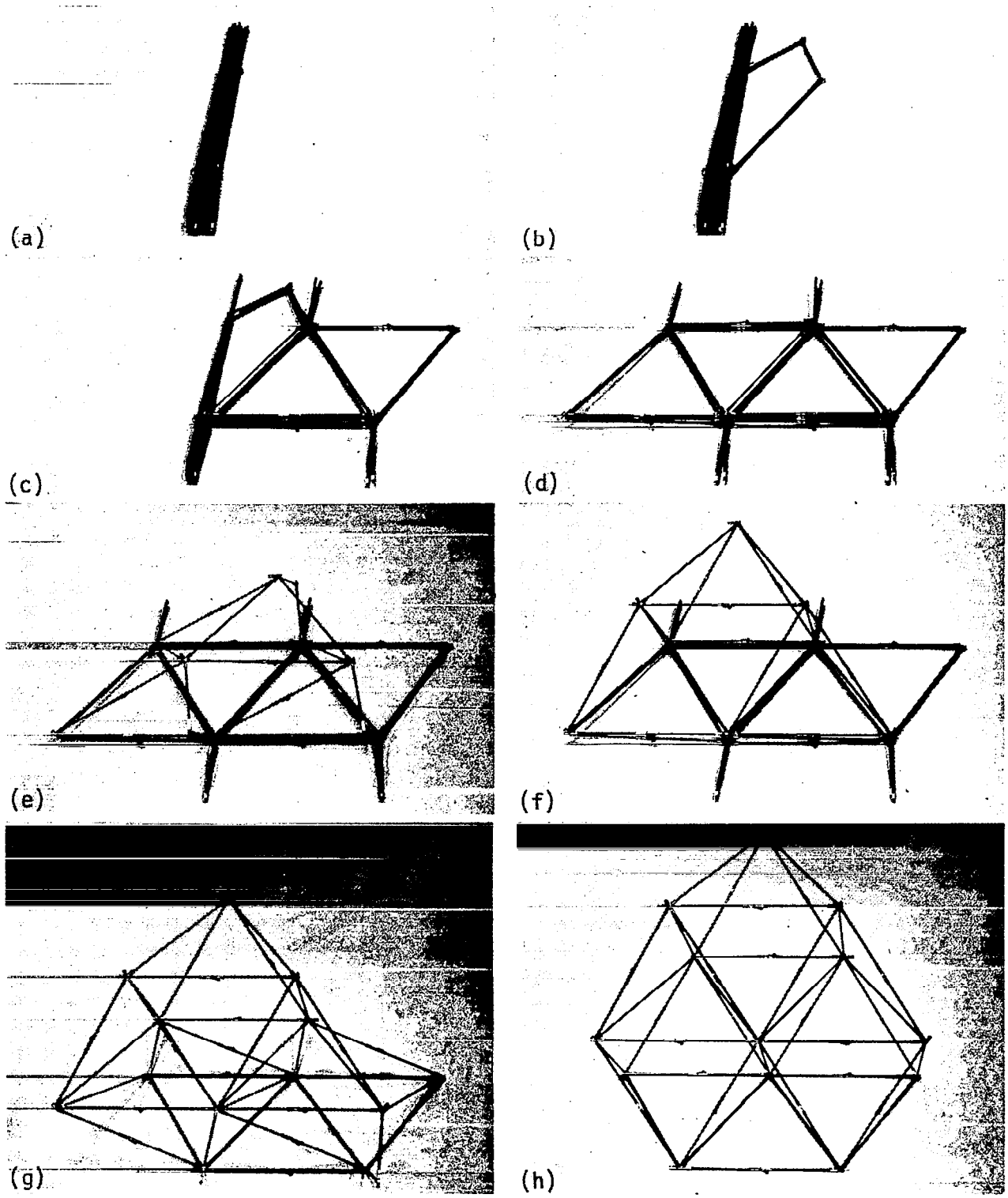

Figure 23. Deployment sequence.

P008

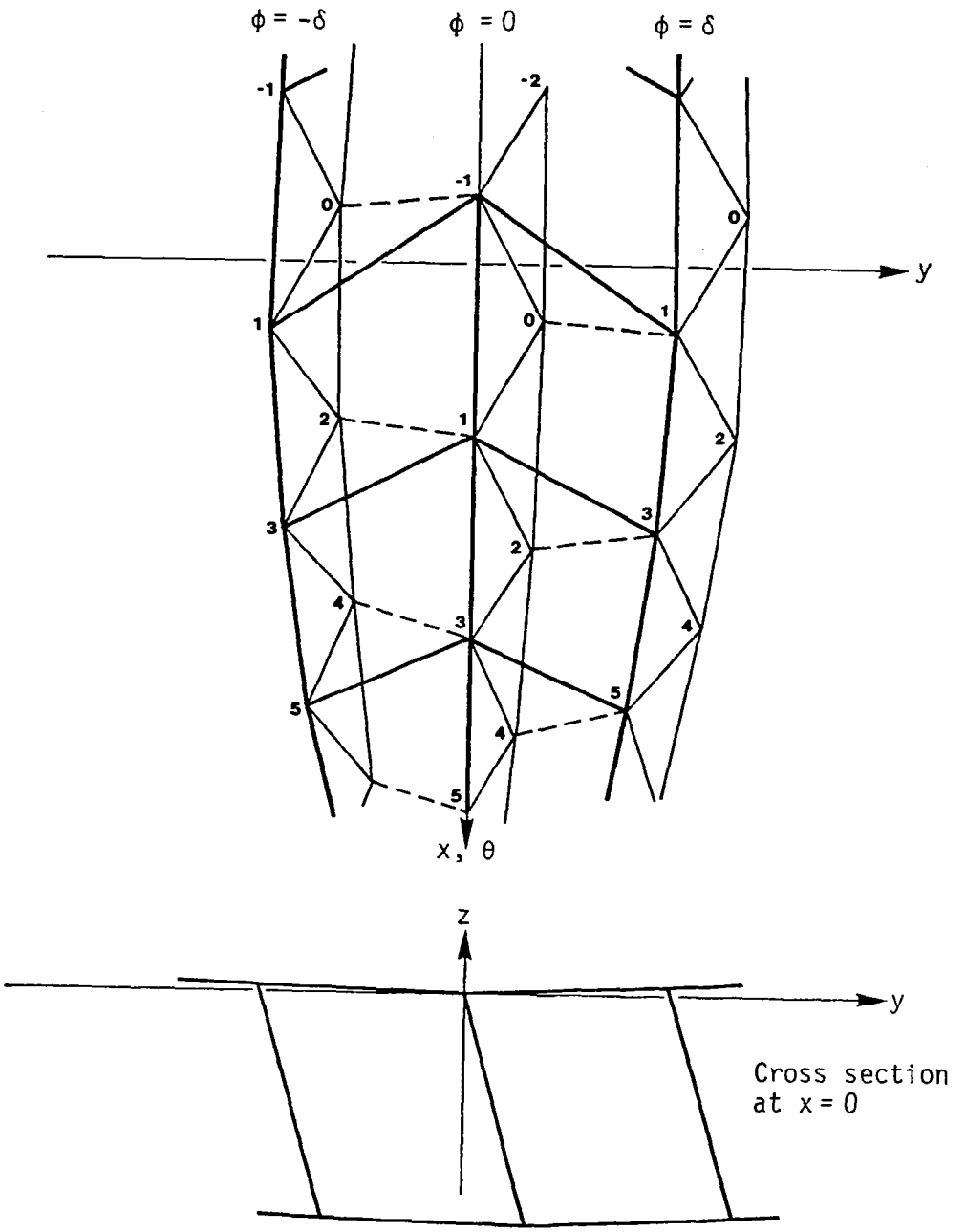

Figure 24. Geometry and nomenclature for doubly curved truss. *006A*

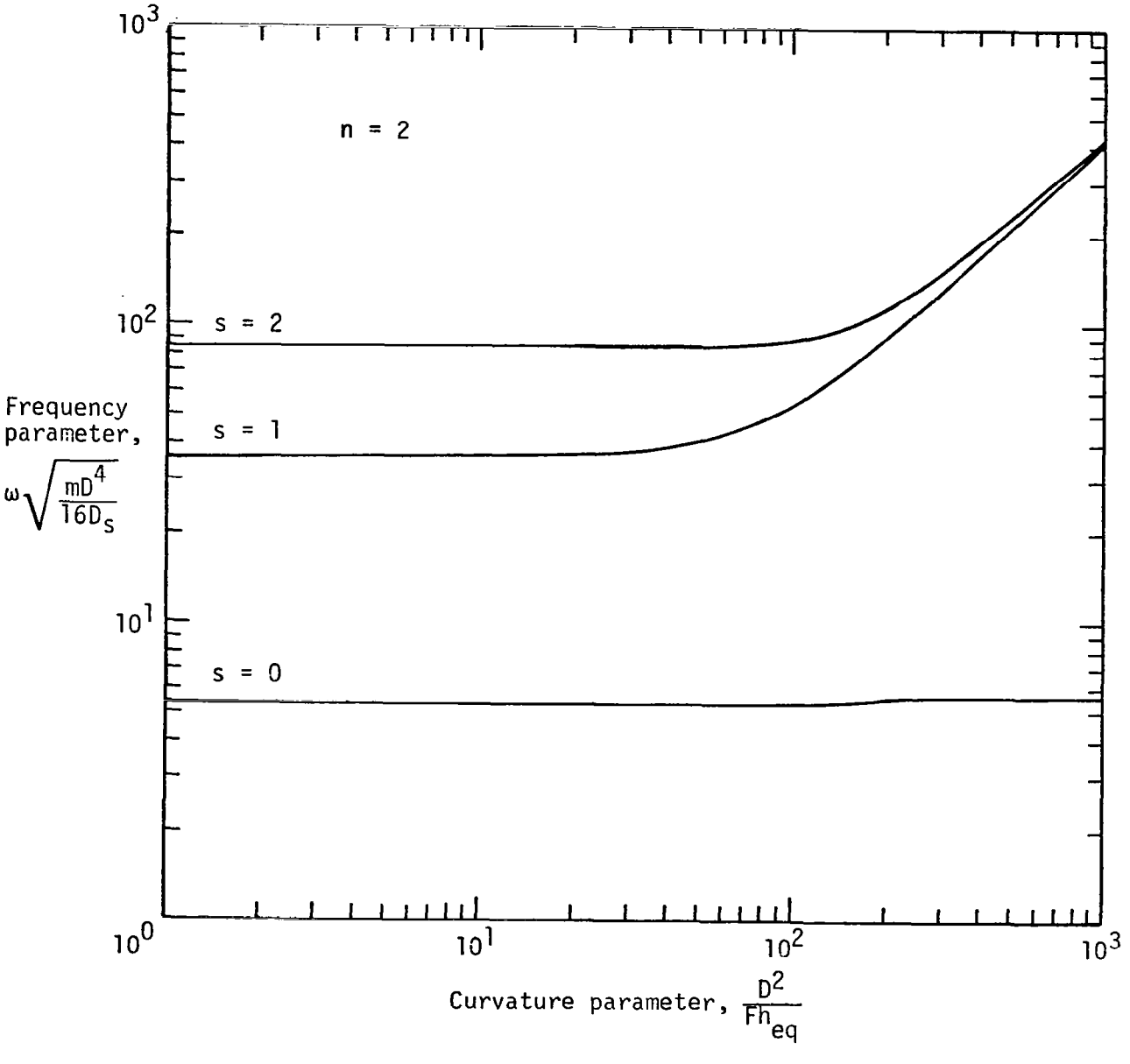

Figure 25. The influence of curvature on the natural frequencies of a shallow spherical shell with a free circular edge for two waves around the circumference (n = 2) and circumferential mode numbers s of 0, 1, and 2. Poisson's ratio ν = 0.33. *007A*

1. Report No.	2. Government Accession No.	3. Recipient's Catalog No.
NASA CR-3663		

4. Title and Subtitle	5. Report Date
DESIGN CONCEPTS FOR LARGE REFLECTOR ANTENNA STRUCTURES	January 1983
	6. Performing Organization Code
7. Author(s)	8. Performing Organization Report No.
John M. Hedgepeth and Louis R. Adams	ARC-R-1018
	10. Work Unit No.
9. Performing Organization Name and Address	
Astro Research Corporation 6390 Cindy Lane Carpinteria, CA 93013	11. Contract or Grant No. NAS1-16134
	13. Type of Report and Period Covered
12. Sponsoring Agency Name and Address	Contractor report
National Aeronautics and Space Administration Washington, D.C. 20546	14. Sponsoring Agency Code

15. Supplementary Notes

Langley Technical Monitor: W. B. Fichter
Final Report

16. Abstract

Practical approaches for establishing large, precise antenna reflectors in space are described. Reflector surfaces consisting of either solid panels or knitted mesh are considered. The approach using a deep articulated truss structure to support a mesh reflector is selected for detailed investigation. A new sequential deployment concept for the tetrahedral truss is explained. Good joint design is discussed, and examples are described both analytically and by means of demonstration models. The influence of curvature on the design and its vibration characteristics are investigated.

17. Key Words (Suggested by Author(s))	18. Distribution Statement
Erectable space structures Large space structures Antenna structures Deployable structures	Unclassified - Unlimited Subject Category 39

19. Security Classif. (of this report)	20. Security Classif. (of this page)	21. No. of Pages	22. Price
Unclassified	Unclassified	82	A05

For sale by the National Technical Information Service, Springfield, Virginia 22161

NASA-Langley, 1983